Stress testing insurance market stability under climate risk

Simona Meiler[1,*], Steven I. Jackson[2], Kerry Emanuel[3], Noah S. Diffenbaugh[4], and Jack W. Baker[1]

[1]Civil and Environmental Engineering, Stanford University, CA, USA
[2]American Academy of Actuaries, Washington, DC, USA
[3]Lorenz Center, Massachusetts Institute of Technology, Cambridge, Massachusetts, USA
[4]Earth System Science, Stanford University, CA, USA
[*]Corresponding author: simona@simonameiler.ch

This manuscript is a non–peer-reviewed preprint submitted to EarthArXiv and currently under review at Science Advances. The content has not yet been certified by peer review and may be subject to change.

ABSTRACT

Extreme weather events exert increasing pressure on communities in hazard-prone areas and on the systems designed to protect them. Insurance serves as a risk-transfer mechanism, providing financial security for homeowners and supporting community resilience. Yet, behind this first layer of protection lies a complex web of reinsurers, capital markets, and public institutions that absorb and redistribute disaster risk. Intensifying climate hazards, continued coastal development, and evolving market dynamics threaten the stability of this network.

Here, we develop a risk-propagation model to assess whether single or sequential tropical cyclones striking Florida could generate systemic financial stress across the property-insurance system. The model links physics-based, probabilistic simulations of tropical cyclone wind and flood losses with data on the Florida residential insurance market, its backstop mechanisms, and regulatory frameworks. By tracing how losses cascade as capital constraints and contractual thresholds bind, we evaluate systemic risk under present-day conditions, future climate scenarios, and alternative market and adaptation configurations within the same quantitative architecture.

We estimate an annual 4% probability that total public burden exceeds 1% of Florida's GDP, indicating that extreme tropical cyclone seasons can overwhelm private market capacity and shift costs to public institutions. Vulnerabilities differ across institutional layers, with post-insolvency mechanisms, residual markets, and the NFIP exhibiting greater sensitivity to extreme and sequential events than formal reinsurance limits. Although we focus on Florida in this proof-of-concept study, this approach provides a transferable template for quantitatively stress-testing insurance systems and evaluating how climate change, market dynamics, and adaptation strategies reshape systemic disaster risk.

Introduction

The 2017 hurricane season (Harvey, Irma, Maria) generated more than USD 260 billion in total losses, or the equivalent of 7–14% of global reinsurers' capital, and absorbed the industry's net income for the year (1). The increasing likelihood of many weather and climate extremes (2) and compound events (3) erodes the stationarity that underpins traditional disaster risk assessment and pricing (4). What was previously manageable year-to-year volatility increasingly reflects systematic changes in hazard characteristics, with implications for long-term planning, capital allocation, and financial stability (5, 6). Disaster insurance transfers losses from households to insurers and state-backed providers, allowing post-disaster repair, supporting mortgage markets, and accelerating economic recovery after extreme events (4, 7). Primary insurers absorb losses up to their capital and reinsurance protection, after which risks propagate to reinsurers, catastrophe bond investors, and public backstops such as state insurance programs or federal institutions. Under moderate shocks, this structure spreads risk efficiently; however, under extreme or clustered events, contractual limits, capital constraints, and regulatory thresholds can bind, causing losses to cascade across institutions rather than being smoothly absorbed (8–10).

In California and Florida, continued urban development (11, 12) and repeated wildfire and tropical cyclone (TC) losses have led to insurer withdrawals, insolvencies, rapid premium increases, and growing reliance on residual or state-backed markets (13–16). In both cases, risk increasingly shifts back to households and public institutions beyond the scale for which these mechanisms were designed, raising concerns that climate-driven disasters may transition from diversifiable shocks to systemic insurance market stress.

Despite growing recognition that climate-driven disasters pose systemic financial risks, insurance markets lack quantitative system-wide stress tests of the kind used to assess stability in banking. In the banking sector, stress testing is a central tool for evaluating the resilience of complex financial systems to rare but severe shocks, focusing on tail risks and the potential for cascading failures (17–19). Climate-related scenario analysis has since been incorporated into prudential supervision, including central bank and regulatory stress-testing exercises (20–22). By contrast, climate risk assessments in insurance have largely centered on catastrophe loss reporting, disclosure frameworks, and firm-level solvency exercises (23–26), which are not designed to quantify when aggregate losses overwhelm market-wide capacity, trigger public backstops, or propagate across interconnected private and public actors. This gap is increasingly consequential as climate change shifts the frequency and clustering of extreme events.

Here, we develop a probabilistic, system-wide stress-testing framework that links physical hazard, market structure, and public backstops to quantify the probability of systemic insurance failure. The framework spans the full set of relevant actors, from primary insurers and reinsurers to capital markets and public institutions, and allows losses to propagate through the system as contractual limits, capital constraints, and statutory thresholds are reached. We apply this framework to the Florida residential property insurance market, where high exposure to TCs, dense coastal development (27), and recent insurer insolvencies (28) following Hurricane Ian in 2022 make systemic risk an immediate concern (10). To stress test this system, we simulate losses from historical TCs (29), stylized sequential events, and large probabilistic event sets representing present-day and future climate conditions (30, 31). We then propagate these losses through the insurance system, and examine how evolving market conditions and adaptation measures modify systemic risk within the same quantitative framework (Fig. 1).

Florida is often described as an early manifestation of climate-related insurance stress that may emerge elsewhere as hazards intensify and exposure grows (10). While institutional details vary across regions and hazards, layered risk transfer across private insurers, capital markets, and public backstops governed by contractual and regulatory thresholds is a common feature of disaster insurance systems. The framework developed here provides a transferable approach for identifying where extreme losses accumulate, under which conditions private capacity is overwhelmed, and how policy interventions reshape systemic risk.

Insurance system architecture and risk propagation

We first summarize the structure of the Florida residential insurance system and the pathways through which TC losses propagate across private insurers, reinsurers, capital markets, and public backstops (Fig. 1c).

In the first layer of risk absorption, losses are distributed between four primary holders of risk: private admitted-market insurers providing wind coverage, Citizens Property Insurance Corporation as Florida's residual wind insurer, the U.S. National Flood Insurance Program (NFIP) providing flood coverage, and households that are uninsured or underinsured. Uninsured and underinsured losses arise both voluntarily, through coverage choices and deductibles, and involuntarily, due to limited insurance availability or policy caps. The NFIP is a federally administered program that offers standardized flood insurance nationwide, while private insurers and Citizens operate at the state level and primarily cover wind-related losses. For each of these entities, we compile exposure data (total insured value and coverage-in-force), which determine how gross TC damages are initially allocated.

In a second layer, we represent formal risk-transfer mechanisms that redistribute insured losses. Private insurers and Citizens purchase reinsurance through the Florida Hurricane Catastrophe Fund (FHCF), a state-run public reinsurance program with company-specific retentions and a statewide seasonal payout cap. Some insurers and Citizens additionally transfer risk to capital markets via catastrophe bonds. The NFIP, by contrast, does not rely on reinsurance; flood claims are paid from the national NFIP pool and, when that pool is insufficient, through borrowing from the U.S. Treasury. At this stage, insured losses are transformed into net losses for each primary insurer after accounting for reinsurance recoveries, cat bond payouts, and regulatory caps.

A final layer captures institutional backstops and loss-sharing mechanisms that activate when insurer capital is insufficient. Insolvent private insurers trigger assessments through the Florida Insurance Guaranty Association (FIGA), which levies assessments on surviving insurers, subject to statutory caps, to cover policyholder claims. Citizens operates under a separate, tiered assessment framework: Tier 1 assessments are levied on Citizens' own policyholders, while Tier 2 assessments can be applied to nearly all property insurance policies statewide, up to prescribed limits. The NFIP has no analogous constraint; losses exceeding the NFIP fund balance are recorded as federal borrowing, effectively transferring flood losses to the national public balance sheet.

We formulate our quantitative systemic risk assessment around this insurance system architecture, evaluating single and sequential historical TCs as well as probabilistic event sets representing present and future climate conditions (Fig. 1b). Across

all simulations, we track the initial loss decomposition across households and insurance entities, the redistribution of losses after risk transfer, insurer capital depletion and defaults, activation of public backstops, and a set of system-level metrics that quantify institutional stress and public burden (Fig. 1d). Full details of data sources, regulatory parameters, and implementation are provided in Section Insurance market data.

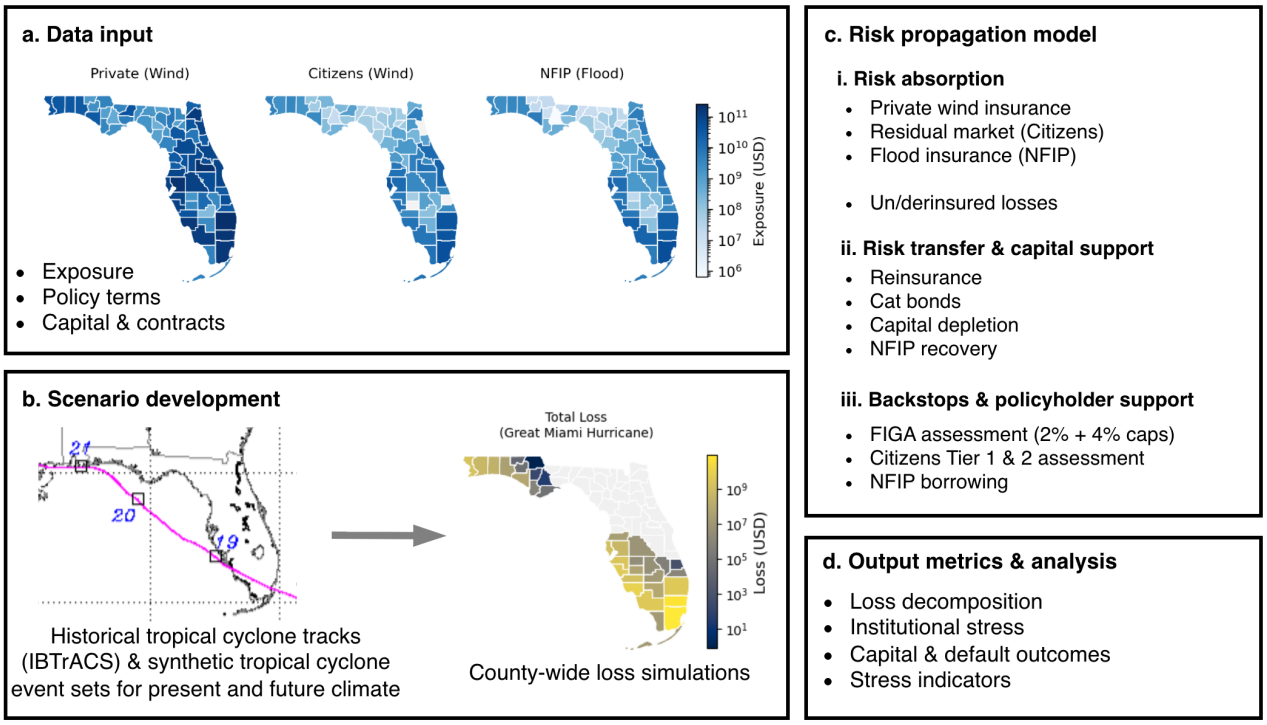

Fig. 1. Insurance system architecture and risk propagation in the Florida homeowners' property insurance market. a) County-level exposure and coverage-in-force for private wind insurers, Citizens Property Insurance Corporation, and the U.S. National Flood Insurance Program (NFIP), together with policy terms, capital positions, and contractual constraints. b) Historical tropical cyclone tracks (IBTrACS) and synthetic event sets representing present and future climate conditions translated into county-level wind and flood loss simulations. c) Loss propagation across three layers: (i) initial risk absorption by insurers, Citizens, the NFIP, and under- or uninsured households; (ii) redistribution through reinsurance, catastrophe bonds, and capital depletion; and (iii) activation of institutional backstops and policyholder assessments, including the Florida Hurricane Catastrophe Fund (FHCF), Florida Insurance Guaranty Association (FIGA), Citizens assessments, and NFIP borrowing. d) Output metrics capturing loss decomposition, insurer capital depletion and defaults, activation of public backstops, and system-level stress indicators under single, sequential, and probabilistic event scenarios.

Results

Stress testing the insurance system with historical and sequential events

We stress test the insurance system using single and sequential historical TC scenarios to examine how extreme losses are distributed across private and public actors. We consider four historically damaging TCs affecting Florida: the Great Miami Hurricane (1926), the Lake Okeechobee Hurricane (1928), Hurricane Andrew (1992), and Hurricane Irma (2017), as well as paired and repeated-event scenarios that probe system behavior under sequential shocks. We evaluate estimated losses from these historical and sequential events on the 2024 exposure and insurance market conditions. Modeled total losses (table S3) fall within the range of published normalized estimates (32, Supplementary Material Table 2), supporting the use of these events as stress-test scenarios.

Across all scenarios, approximately 60-75% of losses remain uninsured or underinsured (Fig. 2a), with the highest shares occurring in flood-heavy events such as the Lake Okeechobee Hurricane and Hurricane Irma, which affect large inland areas with low flood insurance penetration (Fig. 1a, right-most panel). Sequential events (Great Miami followed by Andrew, and Double Andrew) generate particularly large insured losses, exceeding USD 100 billion in aggregate.

Beyond household losses, extreme events impose substantial burdens on public and quasi-public institutions (Fig. 2b). Here, public burden denotes losses that are not covered by private insurer capital, reinsurance, or catastrophe bonds and are instead absorbed through public backstops. These include unrecovered wind losses once the FHCF's statewide seasonal payout cap binds (FHCF shortfall), residual insurer defaults absorbed through FIGA (FIGA residual), deficits exceeding Citizens' surplus and assessment capacity (Citizens deficit), and flood losses financed through borrowing from the U.S. Treasury when the NFIP's fund balance is exhausted (NFIP borrowing). Public burden reaches approximately USD 12 billion for Hurricane Andrew, USD 18 billion for the Lake Okeechobee Hurricane, and USD 26 billion for the Great Miami Hurricane, and increases to USD 50 billion and USD 65 billion for sequential-event scenarios. Notably, the resulting public burden exceeds the sum of the individual-event burdens, even though total losses from sequential events are lower than the combined single-event losses (Fig. 2a), as insured exposure is reduced after the first storm (Section Hazard and loss modeling). This divergence reflects nonlinear amplification of public costs arising from institutional thresholds and payout caps. By contrast, losses from Hurricane Irma are largely absorbed by the initial insurance layers, resulting in minimal total public burden (USD 0.2 billion). Although the FHCF is generally robust and binds primarily for Great-Miami-type or sequential events, FIGA, Citizens, and the NFIP exhibit substantially greater vulnerability, accruing deficits that would require multiple years of premium income to recover (table S3, stress ratios).

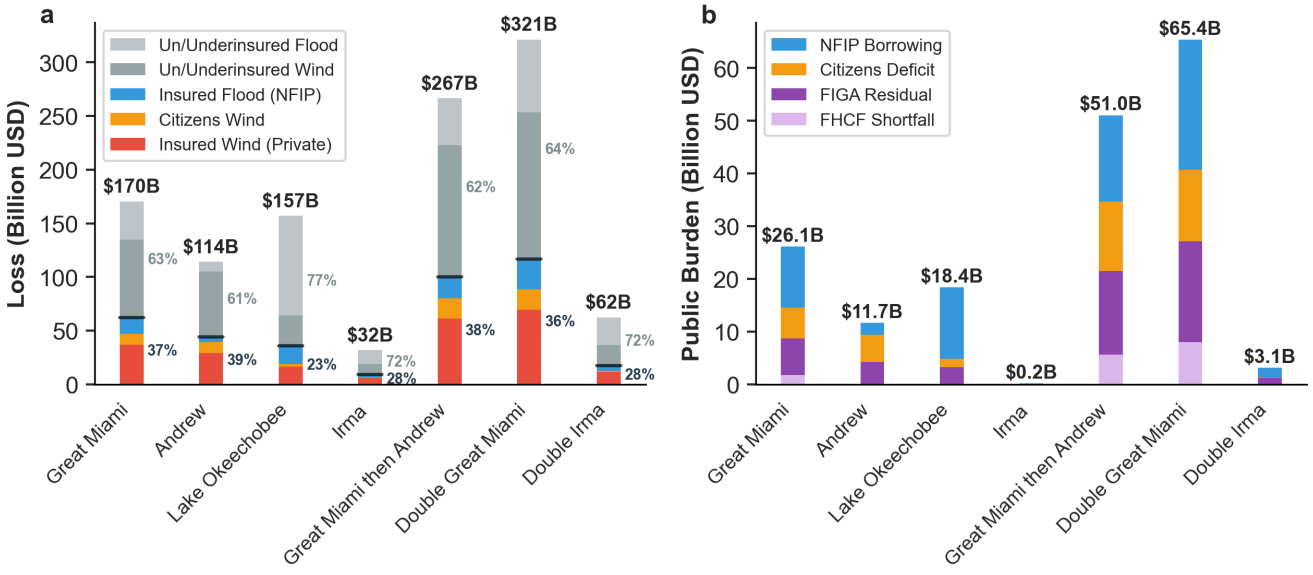

Fig. 2. Loss decomposition and public burden across historical and sequential TC scenarios. a) Decomposition of total losses across insured wind (private market and Citizens), insured flood, and uninsured or underinsured losses. The black horizontal line indicates the split between insured and uninsured losses, with corresponding shares shown numerically. b) Public burden after exhaustion of private insurer capital and risk-transfer mechanisms, apportioned across key public backstops. Total loss and public burden values (USD B) are shown above each bar. All values are shown for single and sequential-event scenarios; a complete tabulation, including uncertainty ranges, is provided in table S3.

Probabilistic assessment of systemic insurance risks

Moving beyond individual scenarios, we quantify systemic insurance risk probabilistically using a catalog of 10 000 simulated TC seasons (Section Hazard and loss modeling). Table 1 places the scenario-based stress tests into a probabilistic context by reporting seasonal return period estimates under present-day climate conditions. A total seasonal loss comparable to the Great Miami Hurricane ($\approx$ USD 170 billion) corresponds to a return period of approximately 35 years under present-day climate and exposure, while the sequential-event scenarios examined above approach the magnitude of a 100-year season. Seasonal and event-based loss return period curves are nearly identical (Figure S1). For example, return period estimates for a Great Miami-scale loss differ by only two years, indicating that aggregation across events within a season does not materially affect tail-loss frequencies in the present-day catalog.

Moreover, the probabilistic results reveal pronounced nonlinear amplification of public burden with increasing loss severity. While total seasonal losses increase by roughly a factor of nine between the 10-year and 100-year seasons (USD 39.5 to 357.2 billion), total public burden increases by over a factor of forty (USD 1.7 to 74.0 billion; Table 1). This supralinear

Table 1. Loss decomposition and public institutional burden across return periods. Return period (RP) estimates are shown for total losses, their decomposition across insured and uninsured components, and the resulting public and quasi-public institutional burden. Public burden reflects residual financial obligations borne by public backstops after exhaustion of private insurer capital and risk-transfer mechanisms.

	Return period [years]						
Metric (USD B)	**10**	**25**	**50**	**100**	**250**	**500**	**1000**
Loss decomposition							
Total loss	39.5	146.9	246.4	357.2	563.9	628.0	738.0
Insured wind – private	11.6	41.8	69.7	103.2	155.2	198.4	214.3
Citizens wind	1.8	6.8	14.5	22.1	35.6	53.6	62.9
Insured flood – NFIP	0.9	3.7	7.4	13.7	26.1	37.6	50.3
Un/underinsured wind	19.8	71.8	125.9	183.1	257.6	321.1	392.1
Un/underinsured flood	3.9	15.1	28.4	47.1	87.3	112.7	141.7
Institutional stress							
Total public burden	1.7	13.9	39.6	74.0	127.7	180.9	214.3
FHCF shortfall	0.0	0.0	6.5	13.7	20.8	26.8	29.6
FIGA residual	1.0	9.2	19.2	32.8	54.9	72.8	80.6
Citizens deficit	0.7	4.5	9.9	17.2	29.3	47.3	57.2
NFIP Treasury borrowing	0.0	0.2	4.0	10.3	22.7	34.1	46.8

scaling reflects exhaustion of private insurer capital, activation of institutional thresholds, and binding payout caps that shift an increasing share of losses to public and quasi-public backstops in the tail of the distribution.

Across return periods, FIGA residuals constitute the largest and fastest-growing component of public burden. At the 100-year season, FIGA residual losses amount to USD 32.8 billion, compared with USD 17.2 billion for Citizens deficits and USD 10.3 billion for NFIP Treasury borrowing, accounting for nearly half of total public burden. FIGA remains the dominant channel through which losses enter quasi-public balance sheets across the full range of return periods considered, whereas FHCF shortfalls remain comparatively limited and occur primarily in more extreme seasons.

The probabilistic approach further allows us to assess the annual exceedance probability of systemic risk thresholds that indicate stress across different components of the insurance system (Fig. 3, table S5). For the private wind insurance market, the annual probability of more than ten insurer defaults is approximately 11%, while the probability that the single largest company deficit exceeds USD 1 billion is around 7%.

For public and quasi-public institutions, the annual probability of exceeding capacity or statutory thresholds differs across entities. The probability that the FHCF reaches its statewide seasonal payout cap remains below 1%, whereas the probabilities of FIGA and Citizens exceeding their respective assessment capacities are approximately 14% and 10%. For the NFIP, the probability that annual losses exceed twice its annual premium income is about 5%. These results mirror the scenario-based findings in Fig. 2, highlighting comparatively greater vulnerability of FIGA, Citizens, and the NFIP relative to the FHCF.

Finally, we relate the aggregate public burden to the economic scale of Florida. The annual probability that total public burden exceeds 1% of Florida's GDP is 3.7%, while the probability of exceeding 10% of state GDP is about 0.1%.

Systemic risk probabilities increase with climate change

We next evaluate how projected changes in TC hazard alter systemic insurance risk under an otherwise fixed present-day insurance architecture, isolating the contribution of climate-driven hazard changes while holding exposure, capital positions, and regulatory parameters constant. Future changes are estimated using a multi-model delta approach that applies the ensemble-median change in each risk metric across CMIP6 simulations to the ERA5-based present-day baseline (Section Future climate scenarios).

Under mid-century scenarios (2041-2060), expected annual total losses approximately double relative to present-day conditions, and expected public burden increases by a factor of approximately three (table S4). Exceedance probabilities of several systemic stress thresholds increase across the private market and post-insolvency channels (Fig. 4, table S5). The annual probability of more than ten insurer defaults rises from 11.4% under present-day conditions to 17.7% (SSP2-4.5) and 18.8% (SSP5-8.5).

Post-default and residual-market mechanisms exhibit particularly strong amplification. The probability that FIGA exceeds its statutory assessment capacity increases from 13.6% to 22.1–23.3%, while Citizens exceeds its assessment capacity with probabilities rising from 9.5% to 15.1–16.1%. In contrast, the probability that the FHCF reaches its statewide payout cap

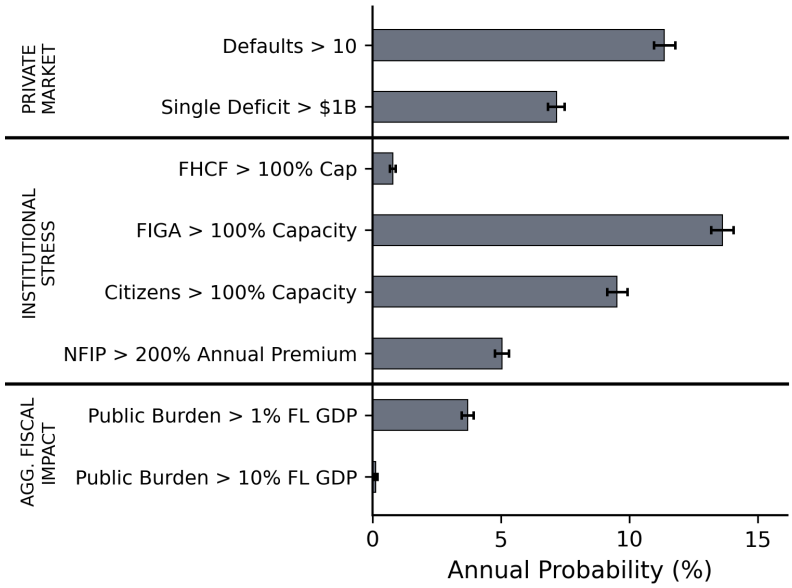

Fig. 3. Probabilistic assessment of systemic insurance risks. Annual exceedance probabilities of predefined systemic stress thresholds across the private insurance market (top), public and quasi-public entities (middle), and aggregate fiscal impact measured as total public burden relative to Florida's GDP (bottom), based on 10 000 simulated tropical cyclone seasons. Bars show mean probabilities with bootstrap confidence intervals (10th–90th percentile) derived from 1000 resamples of the full simulation.

remains at or below 1% across scenarios, and the probability that NFIP annual losses exceed twice premium income increases only modestly (from 5.0% to 5.9–6.1%).

Uncertainty across climate models is substantial in magnitude but does not alter the qualitative direction of change (table S5). For example, under 2050 SSP5-8.5, the probability that FIGA exceeds capacity ranges from 16.6% to 30.9% across the GCM ensemble, compared with a baseline range of 13.2–14.1%. Similar spreads are observed for private insurer defaults (13.1–22.2%, 2050 SSP5-8.5) and Citizens deficits (11.2–20.8%, 2050 SSP5-8.5). At mid-century, differences between emission scenarios are small relative to this inter-model spread (distinct bars in Fig. 4); scenario separation becomes more pronounced by end-of-century but remains smaller than the inter-GCM range.

At the aggregate level, the annual probability that total public burden exceeds 1% of Florida's GDP increases modestly from 3.7% to 4.3–4.5% by mid-century, while exceedance of 10% of GDP remains rare. These smaller macro-fiscal shifts contrast with the stronger amplification observed at the institutional level, indicating that climate-induced stress becomes increasingly concentrated within specific components of the insurance system rather than uniformly expanding aggregate fiscal tail risk.

Systemic risks with evolving markets and insurance policies

We next evaluate how changes in market structure and insurance policies modify systemic risk under present-day hazard conditions. The three stylized interventions represent dynamics currently discussed in policy and industry debates: private-market contraction and expansion of residual markets following recent insolvencies and insurer withdrawals (13, 15, 16); expansion of insurance penetration to reduce protection gaps (10); and strengthened building codes and retrofitting initiatives aimed at reducing physical losses (33, 34). Each intervention modifies a distinct layer of the insurance system architecture while holding all other model components constant (Section Stylized market and policy interventions). Results are shown as changes in annual exceedance probability (percentage points) relative to the ERA5 baseline (Fig. 5).

Private insurer market exit Recent insurer withdrawals and insolvencies have increased reliance on residual markets in several U.S. states (13, 15, 16). To reflect this dynamic, we model a contraction of the private wind market that increases Citizens' market share from 15% to 25% of total insured value, corresponding to a 10% shift of exposure from private insurers, of which 85% transfers to Citizens and 15% becomes uninsured.

Under this scenario, the annual probability of more than ten private insurer defaults declines by about 1.1 percentage points relative to the ERA5 baseline (Fig. 5, table S5), reflecting the reduced exposure and insured loss volume within the

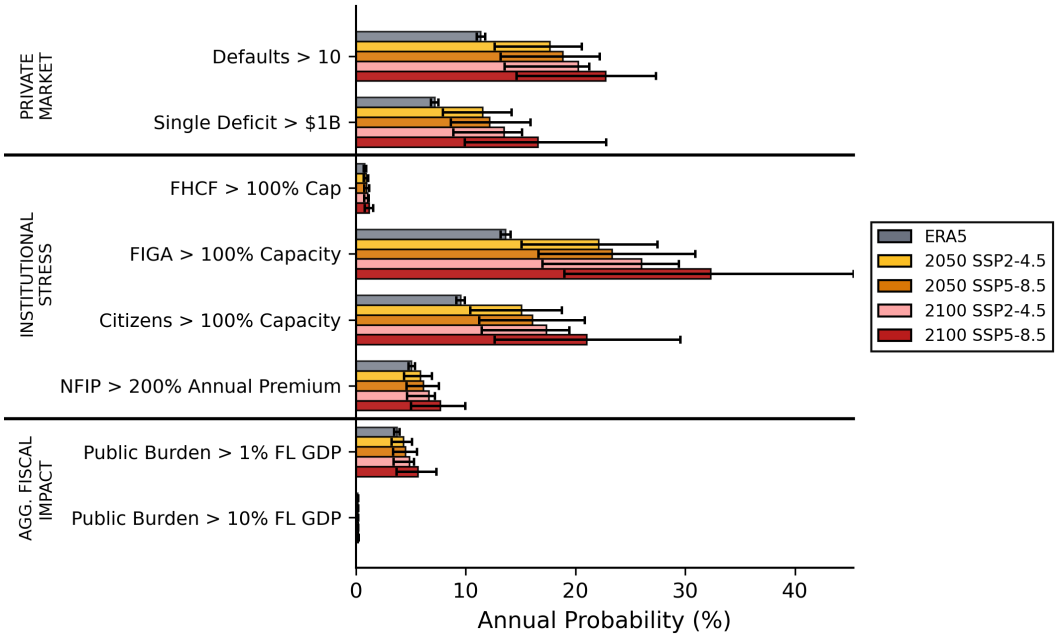

Fig. 4. Probabilistic assessment of systemic insurance risks under future climate scenarios. Annual exceedance probabilities of predefined systemic stress thresholds across the private insurance market (top), public and quasi-public entities (middle), and aggregate fiscal impact measured as total public burden relative to Florida's GDP (bottom), under present-day and future climate conditions. Shown are results for the ERA5 baseline climate (grey), mid-century SSP2-4.5 (yellow) and SSP5-8.5 (orange), and end-of-century SSP2-4.5 (pink) and SSP5-8.5 (red). Bars show mean annual exceedance probabilities corresponding to the median climate-induced risk change across the GCMs used for tropical cyclone track set generation (Section Future climate scenarios), based on 10 000 simulated tropical cyclone seasons; error bars indicate the 10th–90th percentile range across the full GCM ensemble.

private market. However, systemic stress shifts toward residual market mechanisms. The probability that Citizens exceeds its assessment capacity increases by about 3.5 percentage points, while exceedance of the FHCF statewide payout cap remains nearly unchanged (table S5). Expected total public burden rises from USD 2.7 billion to USD 3.1 billion (table S4), and the probability that total public burden exceeds 1% of Florida's GDP increases by around 0.6 percentage points (Fig. 5, table S5).

Insurance penetration increase Efforts to close protection gaps by expanding wind and flood insurance coverage are widely discussed as mechanisms to enhance household resilience (10, 35). To evaluate the systemic implications of higher insurance penetration, we increase wind (from 40% to 60%) and flood (from 11% to 30%) penetration rates, with insurer surplus and NFIP premium volumes scaling proportionally to insured exposure.

While expanded coverage reduces uninsured losses from USD 12.1 billion (combined wind and flood) under baseline conditions to USD 7.8 billion (table S4), its systemic effects are heterogeneous. Several indicators of stress in public or quasi-public institutions increase under higher insurance penetration. Most notably, the annual probability that NFIP losses exceed 200% of annual premium income increases by approximately 4.3 percentage points relative to the ERA5 baseline (Fig. 5, table S5), despite the proportional expansion of the premium base. The probability that Citizens exceeds its assessment capacity increases by approximately 2.3 percentage points, and the probability that total public burden exceeds 1% of Florida's GDP increases by approximately 1.9 percentage points (table S5). Expected public burden rises from USD 2.7 billion to USD 5.1 billion (table S4).

In contrast, several indicators of stress within the private insurance market decline. The annual probability of more than ten private insurer defaults decreases by approximately 1.7 percentage points, while FIGA exceedance decreases marginally by 0.2 percentage points (table S5). These patterns indicate that proportional scaling of capital and premium income does not automatically preserve institutional resilience when insured loss volumes increase (Section Stylized market and policy interventions).

Building code improvement Strengthened building codes and retrofitting initiatives, such as fortified construction standards, reduce structural vulnerability to wind and flood hazards and thereby lower physical damages before losses enter the insurance

system (33, 34, 36). To represent these mitigation effects, we reduce wind-related losses by 30% and flood-related losses by 25% relative to baseline vulnerability prior to allocation across institutional layers.

As a result, exceedance probabilities decline consistently across private, residual, and public components (Fig. 5, table S5). The annual probability of more than ten private insurer defaults decreases by approximately 2.2 percentage points relative to the ERA5 baseline, FIGA exceedance decreases by approximately 2.1 percentage points, and Citizens capacity exceedance decreases by approximately 1.6 percentage points. The probability that total public burden exceeds 1% of Florida's GDP declines by approximately 1.3 percentage points (table S5). Expected total public burden decreases from USD 2.7 billion to USD 1.6 billion (table S4). Unlike the redistribution scenarios above, structural mitigation reduces systemic stress simultaneously across all layers of the insurance architecture.

Taken together, these interventions illustrate how measures acting at different points within the insurance system produce distinct systemic responses. Redistribution of exposure and coverage modifies where stress materializes within the architecture, whereas upstream loss reduction dampens stress across all institutional layers.

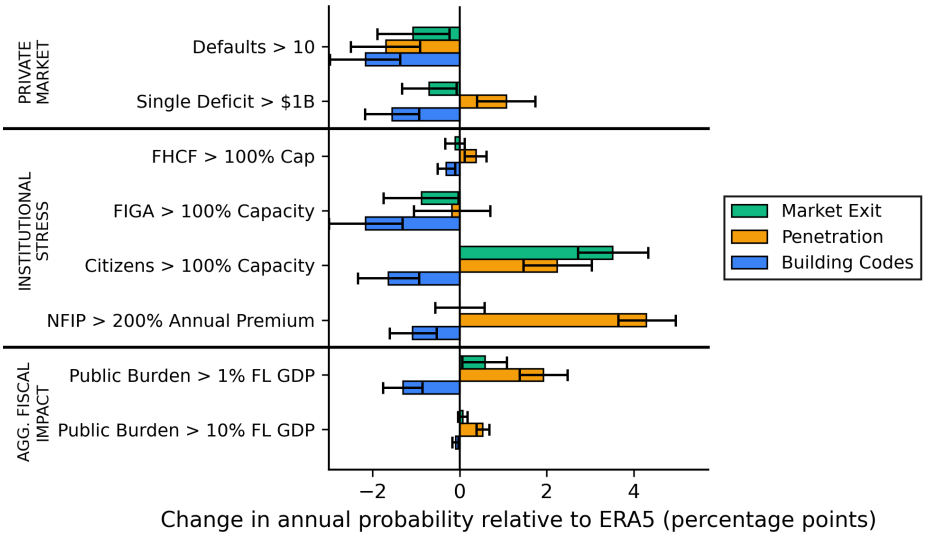

Fig. 5. Changes in systemic insurance risk under stylized market dynamics and insurance policies. Changes in annual exceedance probabilities of predefined systemic stress thresholds across the private insurance market (top), public and quasi-public entities (middle), and aggregate fiscal impact measured as total public burden relative to Florida's GDP (bottom), relative to the ERA5 baseline configuration. Results are shown for three stylized policy scenarios: private insurer market exit (green), increased insurance penetration (orange), and strengthened building codes (blue). Values represent percentage-point changes in annual probability relative to the ERA5 baseline under present-day hazard conditions. Bars show mean changes based on 10 000 simulated tropical cyclone seasons, with uncertainty ranges indicating the 10th–90th percentile. Positive values indicate an increase in the probability of exceeding the corresponding stress threshold relative to baseline, while negative values indicate a reduction.

Building code requirements to offset mid-century climate impacts

We next quantify the level of building code-related loss reduction required to offset projected mid-century climate impacts (SSP2-4.5, 2041–2060) and restore systemic risk metrics to their present-day ERA5 baseline values. Figure 6 shows the sensitivity of annual total losses (a), annual insurer defaults (b), and annual total public burden (c) to increasing building code stringency applied under future climate conditions (Section Building code-climate offset analysis).

For the ensemble median, all three metrics decline monotonically with increasing loss reduction. Annual total losses (Figure 6a) and total public burden (Figure 6c) decrease approximately linearly across most of the loss reduction range, whereas annual insurer defaults (Figure 6b) exhibit a more nonlinear response, with sharper reductions beyond approximately 70% loss mitigation. Restoring annual total losses and insurer defaults to baseline levels requires approximately 70-75% combined wind and flood loss reduction. A similar magnitude of loss reduction is needed to offset increases in annual total public burden, indicating that mid-century climate amplification of fiscal risk closely tracks aggregate loss growth.

Uncertainty across climate models is substantial. For lower-end hazard projections (10th percentile), offsetting current systemic risk levels may be achieved with approximately 30-40% loss reduction, whereas higher-end projections require

substantially stronger loss reduction (approximately 75-80%). These results illustrate that the structural adaptation intensity required to maintain constant systemic risk depends strongly on hazard uncertainty, even within a single emissions scenario. More broadly, this approach enables systematic quantification of the adaptation intensity required to stabilize systemic risk under alternative climate futures within a consistent probabilistic framework.

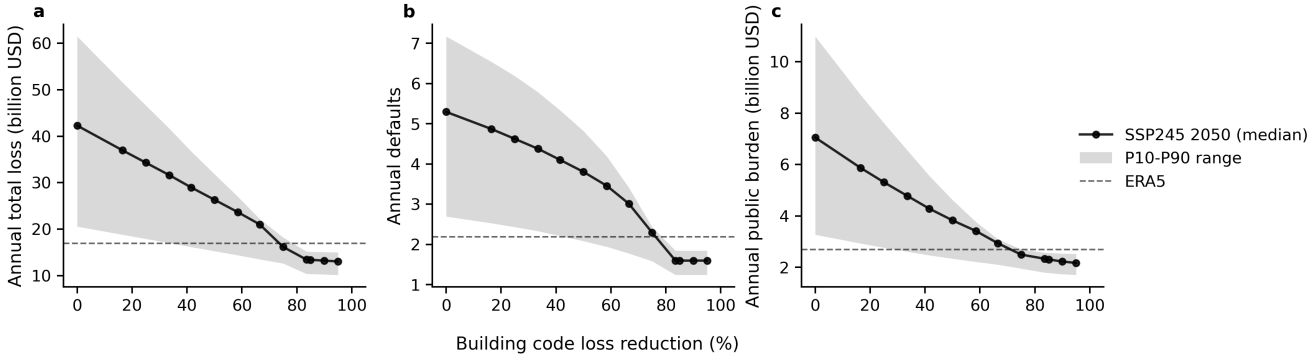

Fig. 6. Sensitivity of systemic insurance outcomes to building code–related loss reductions under future climate conditions. Sensitivity analysis showing the effect of incremental reductions in wind- and flood-related losses resulting from strengthened building codes on systemic risk outcomes under mid-century (2041-2060) SSP2-4.5 climate conditions. Shown are a) annual total loss, b) annual number of private insurer defaults, and c) annual total public burden. Solid lines indicate results for the median climate-induced risk change across the GCM ensemble, shaded bands show the 10th–90th percentile range across GCMs, and dashed lines denote the present-day ERA5 baseline. All quantities represent mean annual outcomes across 10 000 simulated tropical cyclone seasons per climate realization.

Discussion

Public and quasi-public financial burdens scale disproportionately relative to primary disaster losses as institutional thresholds and capital constraints bind. Across probabilistic simulations of Florida's 2024 insurance market, total seasonal losses increase by approximately a factor of nine between 10-year and 100-year return period seasons, while total public burden increases by a factor of over forty (Table 1). Although previous analyses have suggested nonlinear amplification through qualitative scenario exploration (15), our probabilistic framework quantifies the magnitude of this effect.

This amplification of public burden is also unevenly distributed across institutions. The highest systemic stress falls on FIGA, followed by Citizens and the NFIP. The annual probability of exceeding institutional capacity or statutory thresholds reaches 14% for FIGA and 10% for Citizens (Fig. 3). In contrast, the FHCF remains comparatively resilient across baseline, climate change, and market adaptation scenarios, with a consistently low probability of reaching its statutory cap.

The probabilistic framework allows systemic stress to be evaluated across the full loss distribution rather than through isolated disaster scenarios. For example, Andrew-level losses have a return period of less than 25 years under the 2024 Florida market configuration (Table 1). Similarly, insurer defaults are rare in most simulated years but increase rapidly once the first company fails, revealing a strongly nonlinear response of the market to increasing losses.

Because climate change, market structure, and policy interventions are evaluated within the same architecture, policy changes can be traced through the entire insurance system rather than only at the layer where they are implemented. Increasing insurance penetration combined with proportional increases in insurer capital, for example, reduces systemic stress for private insurers but increases stress on public backstop institutions: the probability that NFIP losses exceed multiples of annual premium income rises substantially, while the probability that Citizens exceeds its assessment capacity also increases slightly (Section Insurance penetration increase). Policies targeting one component of the insurance market can thus redistribute systemic risk across institutions rather than uniformly reducing it.

The market dynamics and policy interventions examined here are stylized and designed to probe systemic sensitivity rather than forecast specific outcomes. Empirical evidence suggests that strengthened building codes can reduce hurricane-related wind damage by approximately 30–50% relative to pre-code construction (33, 36). But offsetting increases in systemic risk projected for the mid-century (2050, SSP2-4.5) would require loss reductions of approximately 70–75% under the median hazard scenario. These required reductions exceed empirically observed performance improvements but fall within plausible bounds under less severe hazard realizations within our mid-century ensemble (Fig. 6). The spread across hazard realizations reflects differences in climate sensitivity across the underlying GCMs (37), highlighting that adaptation effectiveness is sensitive

to hazard realization and model uncertainty, suggesting that reliance on a single structural measure is unlikely to suffice under stronger warming. Instead, a portfolio of complementary policy and market interventions may be required to strengthen insurance market resilience.

Our results reflect several modeling choices and data limitations that should be considered when interpreting the findings. Regarding hazards, we use a physics-based TC hazard model with a baseline period of 1980–2023 (30, 31), which may yield higher loss levels than industry models calibrated to longer historical records (38). Wind and flood losses are partitioned using a multi-hazard regression model (39), which is sufficient for probabilistic stress testing but not event-level attribution. Sea-level rise is not explicitly modeled, implying that long-term systemic risks may be conservatively estimated.

On the market side, the 2024 insurance market architecture is fixed across future climate scenarios, isolating the interaction between changing hazard conditions and current institutional structures but not accounting for potential adaptation in underwriting practices, capitalization, or exposure patterns. Future stress estimates should therefore be interpreted as conditional assessments of the present-day market configuration rather than forecasts. Due to lack of alternative data, private insurers' county-level market shares are distributed uniformly from statewide data, likely producing upper-bound estimates of company defaults, and the FHCF is modeled as the sole reinsurance mechanism, omitting additional private reinsurance that could reduce modeled defaults and FIGA assessments. Wind insurance penetration is inferred indirectly and calibrated to approximately 40% in extreme events, which may overstate coverage in smaller events but aligns the model with observed take-up rates in large-loss years that dominate systemic risk outcomes.

By embedding probabilistic hazard realizations within a market-wide representation of insurer capitalization and public backstops, this study provides a quantitative framework for evaluating how climate-driven disaster losses propagate through insurance systems. Our results show that systemic financial exposure can increase nonlinearly with disaster losses, concentrate within specific public backstop institutions, and shift across actors in response to policy and market changes. These findings highlight the importance of system-wide stress testing approaches that capture institutional thresholds and interactions when assessing the financial stability implications of climate risk.

Beyond Florida, the framework developed here provides a template for stress-testing other climate-exposed insurance markets. California's wildfire-prone regions (40) reflect the same layered risk-transfer vulnerabilities shown here, and similar risk-transfer markets govern disaster insurance internationally. A key priority for future research is to trace how uninsured losses propagate into housing markets, credit systems, and public finance, where emerging evidence points to climate-driven debt feedbacks at the municipal level (41) and persistent protection gaps across U.S. flood markets (35). Developing integrated tools that capture these cross-sector feedbacks will be essential for managing climate risk in increasingly interconnected financial and economic systems.

Methods

Data

Insurance market data

Insurance market inputs are anchored to statutory and financial conditions as of 2024, based on insurer statutory filings, regulatory reports, and administrative exposure datasets. Exposure and capital data are harmonized to the county level to ensure consistency with aggregated TC loss estimates and are held constant across simulations.

Exposure and coverage For the private admitted market, total insured value (TIV) by county is obtained from the Florida Hurricane Catastrophe Fund (FHCF) 2024 annual exposure report (42), which provides aggregate residential wind exposure across all participating private insurers. To assign this county-level private TIV to individual insurers, we disaggregate it across the top 100 individual insurers in proportion to their statewide residential direct premiums written for calendar year 2024, as reported in statutory filings (NAIC annual statements, accessed via S&P Capital IQ) and Florida Office of Insurance Regulation (FLOIR) market share reports (43). This procedure preserves observed statewide market structure while ensuring consistency with county-level loss aggregation.

Citizens Property Insurance Corporation's (hereafter, "Citizens'") county-level wind exposure is obtained directly from its published policies-in-force and exposure data as of September 30, 2024 (44). We include all personal residential policy lines, comprising multiperil homeowners and wind-only residential policies.

Flood exposure is based on National Flood Insurance Program (NFIP) coverage-in-force and written premium data for policy year 2024, obtained from the Federal Emergency Management Agency (FEMA) OpenFEMA datasets (45). NFIP participation rates reflect observed take-up inside and outside Special Flood Hazard Areas (46).

Capital and surplus Private insurer capital is measured as statutory surplus as regards policyholders for calendar year 2024, obtained from statutory financial statements filed with the National Association of Insurance Commissioners (NAIC) and accessed via S&P Capital IQ. For insurers affiliated with larger groups, both entity-level and group-level surplus are recorded to allow for potential intragroup capital support within the risk propagation model (Section Capital depletion and intragroup support).

Citizens' surplus as regards policyholders corresponds to its 2024 annual statutory financial statement (47).

NFIP capital consists of the combined National Flood Insurance Fund and Reserve Fund balance of USD 3.441 billion as of October 28, 2024 (CRS Insights IN10784 (48)). Florida-specific annual written premium for policy year 2024, obtained from FEMA OpenFEMA data (45), is used to define exceedance thresholds relative to annual premium income (Section Output metrics and stress indicators).

Reinsurance and catastrophe bonds FHCF contract parameters are based on the 2023-2024 reimbursement contract year. Company-specific coverage elections (45%, 75%, or 90%), reimbursement premiums, and participating insurer identifiers (NAIC codes) are obtained from FHCF coverage selections and premium calculation reports (42). Retention multiples and coverage limits follow the statutory terms reported in the FHCF 2023-2024 annual report (49). Recoveries are subject to the FHCF's season-wide statutory capacity limit of USD 17 billion.

Outstanding catastrophe bonds covering Florida wind exposure active during the 2024 hurricane season are identified using the Artemis deal directory (50) and verified against sponsor offering documents and transaction disclosures. For each bond, we extract sponsor, peril coverage, trigger type (indemnity, industry loss, or parametric), attachment point, exhaustion point, and limit. Bonds are modeled as single-occurrence, single-season layers without reinstatements. Payouts are computed at the sponsor level based on reported attachment and exhaustion terms.

Tropical cyclone track data

We use TC track data from two sources. Historical TC tracks are obtained from the International Best Track Archive for Climate Stewardship (IBTrACS) (29). Synthetic TC tracks are generated using the statistical–dynamical MIT TC model (30, 31).

The model is forced with large-scale environmental fields from the European Centre for Medium-Range Weather Forecasts (ECMWF) fifth-generation reanalysis (ERA5) (51) for present-day conditions and from five CMIP6 global climate models (GCMs) for future conditions under SSP2-4.5 and SSP5-8.5 emission scenarios. The GCMs (CanESM5 (52), CNRM-CM6-1 (53), EC-Earth3 (54), IPSL-CM6A-LR (55), and MIROC6 (56)) span a broad range of global climate sensitivities. Simulations cover three periods: a present-day reference (1980-2023 for ERA5; 1995–2014 for GCMs), mid-century (2041–2060), and late-century (2081–2100). The model was used to generate 200 TCs for each year within these periods using the three-step process of genesis, track, and intensity modeling, yielding a total of 8800 (ERA5) and 4000 (per GCMs) TCs per event set. Annual TC frequency emerges from the fraction of TC seeds used in the genesis step that develop into fully formed

storms (>40 kn) under the prevailing environmental conditions (e.g., potential intensity, vertical wind shear). A frequency bias-correction rescales the number of developed storms relative to the seeded ensemble, ensuring that simulated annual TC counts match the calibrated climatological baseline while preserving climate-driven variability across simulations. This frequency information is used to generate stochastic year sets (Section Hazard and loss modeling) and compute return periods (Section Output metrics and stress indicators).

To focus on Florida-relevant impacts, we retain only TC tracks passing within a 150 km coastal buffer of Florida.

Hazard and loss modeling

We compute county-level TC loss estimates from historical and synthetic TC tracks using the open-source, probabilistic climate risk modeling platform CLIMADA(57), which operationalizes the IPCC risk framework based on hazard, exposure, and vulnerability(58).

First, we use the Holland (2008)(59) parametric wind model to derive a two-dimensional wind field at a horizontal resolution of 120 arc-seconds (approximately 4 km at the equator) from each TC track. The wind model produces the gridded 1-min average sustained winds at 10 m above ground, consisting of a circular wind field component and the translational wind speed generated by the TC's movement. In CLIMADA, the peak lifetime wind speed at each location is used as the hazard variable, disregarding values below 34 kn (17.5 $m\,s^{-1}$). We do not explicitly model TC rainfall or storm surge hazards; their relative contribution to total losses is incorporated through the wind–flood attribution approach described below (Section Wind and flood loss estimation). Sea-level rise projections are not included in future climate TC hazard sets.

Second, we derive a spatially explicit representation of gridded asset exposure values based on the LitPop method (60), which disaggregates national or subnational GDP values to a grid level based on nightlight intensity and population data. The Florida exposure layer used in this study is computed at a resolution of 120 arc-seconds using GDP values (in USD) from 2020.

Third, we use regionally calibrated impact functions (also called vulnerability functions) that relate hazard intensities to relative economic damage ratios (61) to compute event-based loss estimates. The regional calibration was conducted for nine global regions of differing socio-demographic composition and vulnerability. Here, we apply the USA-specific impact function to represent macroeconomic TC losses at the state scale; sub-county variations in structural vulnerability are not explicitly modeled, consistent with the system-level focus of this analysis. Although parameterized by wind intensity, the impact functions were calibrated to observed total TC losses and therefore capture the aggregate effects of wind, rainfall, and storm surge.

The resulting total loss estimates for historical TCs (1926 Great Miami Hurricane, 1992 Hurricane Andrew, 1928 Lake Okeechobee Hurricane, and 2017 Hurricane Irma; table S1) fall within the range of normalized loss estimates reported in the literature (32, Supplementary Material Table 2). For the historical scenario-based insurance market stress test, we construct sequential-event scenarios by combining individual TCs: Great Miami followed by Andrew, Great Miami twice, and Irma twice. Losses are computed sequentially to account for reductions in exposed asset values after the first event. We do not model potential changes in vulnerability between events due to limited empirical evidence. These sequential scenarios should therefore be interpreted as stylized stress tests that capture exposure depletion but do not incorporate additional compounding or dynamic recovery effects.

Because the insurance market operates on county-level exposure portfolios, event-based gridded losses are aggregated to county totals, which form the direct input to the financial risk propagation model (Section Insurance market data).

Loss estimates from the synthetic TCs are used to construct stochastic event sets spanning 10 000 simulated years. From the 8800 ERA5-based and 4000 GCM-based simulated events in each TC event set, annual TC seasons are generated by sampling events with replacement according to the TC event set-specific annual frequency (Section Tropical cyclone track data). This procedure yields years without TC losses (ERA5 baseline: 28.5%), years with a single event (15.3%), and years with multiple events (56.2%). These synthetic year sets form the basis of the probabilistic systemic risk assessment.

Wind and flood loss estimation Because the systemic stress test requires separate accounting of wind and flood losses within the insurance market structure (Section Layer 1: Risk absorption), total TC losses must be decomposed into sub-hazard components. Explicit simulation of rainfall- and surge-driven losses using dedicated hazard models would be computationally intensive and require additional impact-function calibration and multi-peril loss modeling, for which event-level empirical data separating wind and flood damages remain limited. Instead, we adopt a pragmatic and physically informed wind–flood attribution approach based on an external multi-hazard damage regression model.

Specifically, we partition total economic TC losses simulated in this study (Section Hazard and loss modeling) into wind and flood components using the multi-hazard regression model of Gori et al. (2025)(39, 62). That study combines county-level wind, rainfall, and storm surge intensities derived from physics-based hazard models with a regression-based damage model calibrated on observed disaster losses. Because the TC simulations in Gori et al. (2025) originate from the same underlying statistical–dynamical TC track model used here (30, 31), their hazard dataset provides a consistent basis for estimating relative wind and flood contributions.

For each TC event e and county c, we construct a compound hazard metric

$$H_{e,c} = \beta_V V_{\max,e,c} + \beta_P P_{\mathrm{cum},e,c} + \beta_S S_{\max,e,c}, \tag{1}$$

where regression coefficients β_V, β_P, and β_S follow the regional specification of Gori et al. (2025)(39). To focus on high-intensity hazard realizations most relevant for systemic loss and insurance stress, we restrict the analysis to the upper 95th percentile of $H_{e,c}$ across all modeled events. Within this subset, we compute county-level hazard contribution ratios

$$r_{V,c} = \frac{\beta_V \langle V_{\max,c} \rangle_{p95}}{\beta_V \langle V_{\max,c} \rangle_{p95} + \beta_P \langle P_{\mathrm{cum},c} \rangle_{p95} + \beta_S \langle S_{\max,c} \rangle_{p95}}. \tag{2}$$

Aggregation across Florida's exposure-weighted counties yields a state-wide wind attribution of 84.6% (flood: 15.4%, comprising 10.2% surge and 5.2% precipitation).

For each simulated event, an event-level wind share is sampled from a Beta prior (event-specific for historical benchmark events; otherwise from a default prior centered at 84.6% wind). Total county loss is then partitioned into wind and flood components using county-specific empirical wind shares, after proportional rescaling so that the loss-weighted state-wide mean exactly equals the sampled event-level wind share. Flood loss is defined residually as the complement of wind loss.

$$L_{V,e,c} = L_{\mathrm{total},e,c}\, r_{V,e,c}, \qquad L_{F,e,c} = L_{\mathrm{total},e,c}\,(1 - r_{V,e,c}). \tag{3}$$

Here, $r_{V,e,c}$ denotes the rescaled county-specific wind fraction for event e.

For the historical benchmark scenarios (1926 Great Miami Hurricane, 1992 Hurricane Andrew, 1928 Lake Okeechobee Hurricane, and 2017 Hurricane Irma), the event-level prior means are set from literature-based damage reconstructions (70%, 87.5%, 30%, and 50%, respectively), with Beta priors used to represent epistemic uncertainty.

Risk propagation model

The risk propagation model translates county-level TC wind and flood losses into entity-specific financial impacts and traces how losses cascade through private insurers, reinsurance arrangements, capital markets, and public backstops. The model is organized into three sequential layers: (1) initial risk absorption, (2) formal risk transfer and capital depletion, and (3) public backstop mechanisms (Fig. 1c). At each stage, losses are reallocated according to contractual provisions, statutory limits, and observed capital structures (Section Insurance market data).

Layer 1: Risk absorption

For each event, modeled gross wind and flood losses (Section Wind and flood loss estimation) are partitioned into insured and uninsured components. For wind losses, we calibrate the insured fraction using an empirical reconstruction approach consistent with the U.S. Billion-Dollar Disaster Database methodology (63, 64), in which total economic losses are inferred from insured losses, NFIP payments, and federal disaster assistance. Combining Florida-specific insured loss data from the Florida Office of Insurance Regulation (2017–2024) (65) with NFIP payouts (66) and federal disaster assistance (67), we estimate annual insured shares of total economic losses. To account for uncertainty in the treatment of federal disaster assistance, we compute insured shares using formulations both including and excluding public disaster aid and take the average across approaches. The resulting distribution indicates that insured shares increase with event severity and approach approximately 40% for high-loss events (Supplementary Methods). Because our stress-test scenarios focus on severe hurricane events and seasons, we represent uncertainty in the insured wind fraction using a Beta(4,6) distribution centered at 0.4. The residual share of wind losses remains on household balance sheets and does not enter the insurance system. Sensitivity analysis indicates that the assumed insured wind fraction materially affects systemic-risk outcomes. Reducing the fixed insured fraction from 0.4 to 0.1 lowers the mean FIGA residual deficit by 88% while increasing uninsured and underinsured household wind losses by 50% (table S4). Backstop-mechanism outcomes respond more than proportionally to changes in the insured fraction because a higher insured fraction routes more wind losses through insurer balance sheets, elevating default risk and, in turn, amplifying downstream FIGA, Citizens, and group-capital shortfalls.

For flood losses, the insured fraction is determined using county-level NFIP take-up rates (46), accounting for participation inside and outside Special Flood Hazard Areas. Insured flood losses are capped by aggregate county coverage-in-force, and payouts are modeled on a dollar-for-dollar basis up to policy limits. Residual flood losses represent uninsured household burdens.

Insured wind losses are allocated to private insurers and Citizens in proportion to their county-level exposure shares, measured by TIV. Insured flood losses are assigned to the NFIP (Section Insurance market data). This allocation establishes each entity's gross insured loss before reinsurance recoveries or capital adjustments.

Layer 2: Risk transfer and capital support

Reinsurance and catastrophe bonds Insured wind losses are partially redistributed through the FHCF, a state-run public reinsurance program with entity-specific retention levels, coverage percentages, and aggregate limits. For each insurer, recoverable losses are defined as insured wind losses exceeding its retention up to its contractual cap. Recoveries are computed by applying the selected coverage percentage (45%, 75%, or 90%) and a 10% loss adjustment expense factor.

Aggregate FHCF payouts across all participating insurers are constrained by a statewide seasonal cap of USD 17 billion. When modeled recoveries exceed this threshold, individual recoveries are proportionally scaled to satisfy the cap. Resulting net wind losses equal insured wind losses minus FHCF recoveries.

An additional layer of risk transfer is provided by catastrophe bonds covering Florida wind exposure. Bonds are modeled as single-occurrence, single-season layers without reinstatements. For indemnity bonds, payouts are determined by comparing sponsor-specific post-FHCF net losses to attachment points and applying bond limits. For index or industry-trigger bonds, payouts are based on statewide insured wind losses prior to FHCF recovery. Catastrophe bond payouts reduce insurer net losses but do not modify FHCF mechanics or its seasonal cap.

Insured flood losses are financed through the NFIP. Modeled payouts first draw on the national NFIP fund balance. Losses exceeding available reserves are recorded as borrowing from the U.S. Treasury, consistent with statutory backstop authority, thereby transferring residual flood losses to the federal balance sheet.

Capital depletion and intragroup support Net wind losses remaining after reinsurance and capital-market recoveries are applied to each insurer's statutory surplus as regards policyholders. Insurers with negative post-loss surplus are considered insolvent unless supported by an affiliated insurance group.

Using NAIC group identifiers, insurers are organized at the parent-group level. Group-level excess capital is defined as total group surplus minus the sum of member statutory entity surpluses, floored at zero. Intragroup support is permitted only for distressed statutory entities belonging to groups with a Group-to-Entity surplus ratio greater than 10, representing material group-level capital buffers. Eligible distressed entities are assumed to receive capital support sufficient to restore non-negative surplus, funded from available group excess capital without reducing supporting entities below zero surplus. Insurers without group affiliation, or belonging to groups below the eligibility threshold, receive no support. Residual shortfalls after potential group contributions determine insolvency status and transition losses to institutional stabilization mechanisms.

Layer 3: Public backstops

When private capital buffers are exhausted, residual losses transition to statutory stabilization mechanisms. Insurers with negative surplus after accounting for potential intragroup support are declared insolvent. Resulting deficits are transferred to the Florida Insurance Guaranty Association (FIGA), which finances policyholder claims through assessments on surviving insurers subject to statutory limits (2% normal assessments and up to 4% emergency assessments of premium volume). If aggregate deficits exceed FIGA's maximum assessment capacity, the remaining shortfall is recorded as residual policyholder loss.

Citizens' net wind losses are applied to its surplus. When surplus is insufficient to absorb losses, Citizens activates its statutory two-tier assessment authority. Tier 1 assessments are levied on Citizens policyholders (up to 15% of premium base), followed by Tier 2 assessments on nearly all Florida property insurance policies (up to 10% of statewide premium base). Any deficit remaining after both assessment tiers are exhausted represents residual public burden.

Simulation design and probabilistic assessment

The risk propagation model is evaluated in two complementary settings: event-based stress tests and probabilistic seasonal simulations. First, we apply the model to individual historical events and constructed sequential-event scenarios, performing 200 Monte Carlo iterations per event to capture parametric uncertainty while holding event characteristics fixed. Second, we conduct a probabilistic assessment using 10 000 synthetic TC seasons, each representing a stochastic realization of annual event occurrence and associated financial parameters.

For each realization, county-level wind and flood losses are propagated through the deterministic financial structure described above. Uncertainty arises from both variation in synthetic event realizations and parameter sampling, including insured wind fractions (Beta(4,6)), wind–flood damage shares represented as Beta-distributed priors (event-specific for historical benchmark events and otherwise a default prior centered at 84.6% wind; Section Wind and flood loss estimation), and stochastic perturbations of total insured values (coefficient of variation 0.15). In probabilistic assessment, outcome variability is primarily driven by differences in synthetic event realizations rather than parameter perturbations. We verify this with a nested Monte Carlo variance decomposition: 300 seasons sampled across the loss distribution — ensuring they span the full range of losses rather than being randomly drawn — are each replayed 50 times with independent parameter draws, and a one-way ANOVA statistic η^2 measures the fraction of total variance attributable to between-season (hazard) differences. Hazard realization explains $\geq 73\%$ of variance across all output metrics, and $\geq 95\%$ for all metrics except those linked to flooding.

For flood-related metrics, the remaining $\sim 25\%$ parameter contribution arises from the wind/water share Beta prior, which determines how much of total damage is routed to NFIP versus private wind coverage (table S5). The propagation logic remains identical across simulations.

Output metrics and stress indicators

Model outcomes are evaluated using metrics designed to quantify (i) loss decomposition across primary risk absorption entities, (ii) institutional stress within the insurance system, (iii) capital depletion and default dynamics, and (iv) system-level fiscal impacts. Formal definitions of all metrics are provided in table S2.

For each event or simulated season, total economic losses are decomposed into insured wind losses (private insurers and Citizens), insured flood losses (NFIP), and uninsured household losses. This decomposition characterizes the insurance protection gap and the initial distribution of gross damages across private and public balance sheets.

Institutional stress for public and quasi-public entities is quantified relative to their binding statutory or contractual limits as implemented in the risk propagation model. For each event or simulated season, we report realized institutional stress totals (FHCF reimbursements, FIGA deficits, Citizens assessment utilization, and NFIP borrowing). Within the probabilistic simulations, we additionally compute annual exceedance probabilities of key capacity thresholds, including the FHCF seasonal aggregate cap (USD 17 billion), FIGA's maximum assessment capacity (2% normal plus up to 4% emergency assessments of surviving property insurers' written premium), Citizens' combined Tier 1 (15% of Citizens premium base) and Tier 2 (10% of statewide property premium base) assessment authority, and NFIP insured losses exceeding twice its annual premium income. All parameters reflect 2024 statutory conditions and are held constant across simulations.

Private-sector stress is measured through post-loss surplus positions after reinsurance recoveries, catastrophe bond payouts, and potential intragroup capital support. We record the number of insurer insolvencies and the largest single-entity deficit. These indicators capture the extent to which losses exceed available private capital buffers.

At the system level, we define total residual public burden as the aggregate fiscal exposure that remains after private capital buffers and statutory institutional capacities are exhausted. This measure combines FHCF reimbursement shortfalls, FIGA and Citizens deficits beyond assessment authority, and NFIP borrowing requirements. We compute annual exceedance probabilities of total public burden relative to Florida state GDP (e.g., >1% and >10%) and derive empirical return periods for total losses and aggregate public-sector burdens across simulated year sets.

Empirical return periods are computed from probabilistic TC event sets by ranking outcomes in descending order, calculating their cumulative exceedance frequency based on simulated event or seasonal frequencies, and defining the return period as the inverse of this exceedance probability. For seasonal analyses, frequencies correspond to simulated year sets (10 000 stochastic seasons); for event-based analyses, they reflect the modeled annual frequency of individual storms (Section Hazard and loss modeling).

Climate change and insurance market configuration experiments

Future climate scenarios Future TC projections are generated using the statistical–dynamical MIT TC model (30, 31) forced by environmental fields from CMIP6 global climate models (Section Tropical cyclone track data). We then evaluate how projected changes in TC activity translate into systemic insurance risk using a multi-model ensemble approach. Rather than using GCM-driven simulations directly to estimate future risk levels, we add climate change deltas to the ERA5 baseline. This delta approach, which is standard in the climate impact literature, avoids systematic low biases in TC intensity that arise when synthetic storms are generated from the lower-resolution environments of global climate models (31, 68).

For each GCM m, scenario s, time period t, and systemic risk metric i, we compute absolute deltas relative to that GCM's historical reference period:

$$\Delta^{\text{abs}}_{m,s,t,i} = \text{Value}^{\text{future}}_{m,s,t,i} - \text{Value}^{\text{hist}}_{m,i}. \tag{4}$$

For each scenario–period–metric combination, deltas are aggregated across the five-GCM ensemble to obtain the median and 10th-90th percentile range. These ensemble deltas are then added to the ERA5-based baseline metrics:

$$\text{Value}^{\text{scaled}}_{s,t,i} = \text{Value}_{\text{ERA5},i} + \Delta^{\text{abs}}_{s,t,i}. \tag{5}$$

This formulation isolates the modeled climate change signal while preserving the observationally constrained baseline risk distribution derived from ERA5-driven simulations.

For continuous outcome metrics (e.g., total losses, institutional burden), scaled values are computed directly using the additive delta. However, several key systemic indicators are expressed as annual exceedance probabilities of binary events (Section Output metrics and stress indicators). For a binary outcome B, the baseline annual probability is defined as

$$P_{\text{baseline}}(B) = \frac{1}{N} \sum_{j=1}^{N} \mathbb{1}[B_j], \tag{6}$$

where $N = 10\,000$ is the number of simulated years and $\mathbb{1}[\cdot]$ is the indicator function.

Future exceedance probabilities are estimated using a conservative square-root scaling:

$$P_{\text{future}}(B) = \min\left(P_{\text{baseline}}(B)\sqrt{\lambda}, 0.999\right), \tag{7}$$

where $\lambda = \text{Value}^{\text{scaled}}{s,t,i}/\text{ValueERA5},i$ is the scenario- and period-specific scaling factor of the corresponding continuous driver of the exceedance event. The square-root transformation reflects the nonlinear relationship between shifts in loss distributions and threshold exceedance probabilities, while the upper bound prevents numerical artifacts.

For composite indicators (e.g., total residual public burden combining multiple institutional shortfalls), scaling factors are computed as the ensemble-average scaling across the contributing continuous components.

Uncertainty in future projections reflects both baseline sampling variability and inter-GCM spread in climate deltas. Baseline Monte Carlo uncertainty is quantified via bootstrap resampling (1000 iterations) of the 10 000-year ERA5 simulations, yielding 10th–90th percentile confidence intervals. Climate change uncertainty is represented by the 10th-90th percentile range of deltas across the five GCMs. These uncertainty bounds are propagated consistently to all reported future risk metrics.

Stylized market and policy interventions We evaluate three stylized insurance market interventions representing distinct dynamics and adaptation strategies within the Florida insurance system: (i) private-market contraction ("market exit"), (ii) expanded insurance penetration and depopulation of Citizens ("penetration"), and (iii) strengthened building codes and retrofitting ("building code"). Each scenario modifies specific components of the insurance system architecture while holding all other model parameters constant throughout the 10 000 simulated years, enabling isolation of intervention effects on systemic risk metrics.

Private insurer market exit. We model a private insurance market contraction that increases Citizens' market share from 15% (baseline) to 25% of total insured value, corresponding to a 10% shift of exposure from private insurers. Of the exited private exposure, 85% transfers to Citizens and 15% becomes uninsured. Private insurers' surplus levels are reduced in proportion to their exposure contraction, assuming partial retention of fixed capital, while Citizens' surplus requirement scales with market share to the power of 1.2, implying an 84% increase in required surplus for a 66.7% increase in exposure. Gross wind and flood losses remain unchanged; only the pre-event allocation of exposure and capital across entities is modified. The intervention therefore redistributes financial burden without altering physical damages, increasing concentration risk within Citizens and reducing aggregate private capital buffers.

Insurance penetration increase. We model an expansion of insurance coverage and depopulation of Citizens. Wind insurance penetration increases from 40% to 60% of insurable value, and flood insurance penetration from 11% to 30%. Flood penetration increases are implemented using county-level FEMA data distinguishing SFHA and non-SFHA areas (46). Baseline penetration rates of approximately 35% within SFHAs and 5% outside SFHAs are scaled by factors of 1.2 and 3.0, respectively, yielding an overall statewide increase from 11% to 30%. Coastal counties receive 1.5× larger proportional increases than inland counties. NFIP policy counts, coverage amounts, and premium volumes are adjusted proportionally. Concurrently, Citizens' market share decreases from 15% to 8% through active policy transfers to private insurers and higher proportional expansion of private market exposure. Insurer surplus levels scale proportionally with exposure growth. Gross wind and flood losses are unchanged; however, the insured fraction of losses increases and the uninsured household burden decreases. This intervention expands the premium base and shifts loss absorption toward the private market, while reducing Citizens' exposure.

Building code improvement. We model structural loss reduction through enhanced building standards and retrofitting that reduce wind-related losses by 30% and flood-related losses by 25% relative to baseline vulnerability. Loss reductions are applied to wind and flood loss estimates before allocation into insured and uninsured components. Exposure values and insurer capital levels remain unchanged. Unlike the previous two interventions, this scenario reduces total losses rather than reallocating them.

Building code–climate offset analysis We conduct a sensitivity analysis to determine the level of building code improvement required to offset projected mid-century climate change impacts (SSP2-4.5, 2041–2060) and maintain systemic risk levels that exist in the current climate. Using the same Future climate scenarios approach described above, we simulate historical (1995–2014) and future (2041–2060) conditions with 10 000 synthetic years per model. For the future period, we evaluate 13 building code levels representing combined wind and flood loss reductions ranging from 0% to 95%, with wind and flood reductions applied in a fixed 3:2 ratio.

For each GCM m and building code level b, we compute the climate delta for systemic risk metric M as

$$\Delta_{m,b}(M) = \overline{M}_m^{\text{future},b} - \overline{M}_m^{\text{historical}}, \tag{8}$$

where $\overline{M}$ denotes the sample mean of metric M computed across 10 000 simulated years, with building code reductions applied only to the future scenario. Ensemble median and 10th–90th percentile deltas across the five GCMs are then added to the ERA5 baseline.

Data availability

Data used in this study are available from the sources cited in the Methods section. Data from S&P Capital IQ require a commercial license and are not publicly accessible.

The synthetic TC data from the MIT model are proprietary and owned by WindRiskTech L.L.C., a company that provides hurricane risk assessments to clients worldwide. Due to proprietary restrictions, these datasets are not publicly archived. However, researchers interested in accessing the data for scientific purposes can contact WindRiskTech L.L.C. at info@windrisktech.com, subject to a non-redistribution agreement.

Code availability

For this study, we used the Python (version 3.11+) version of CLIMADA, release v6.1.0-dev (69). Source code is openly and freely available under the terms of the GNU General Public License Version 3 (57).

Code to reproduce the results of this paper is available at a GitHub repository (70) with the identifier 10.5281/zenodo.19361128.

References

1. Swiss Re Institute, 2017: Hurricanes and the impact on the reinsurance market | Swiss Re. https://www.swissre.com/institute/research/topics-and-risk-dialogues/climate-and-natural-catastrophe-risk/topic-hurricanes-and-the-impact-on-the-re-insurance-market.html, Accessed on 2026-02-20.
2. Seneviratne, S. I., M. G. Donat, A. J. Pitman, R. Knutti, L. J. Wilcox, and X. Zhang, 2021: Weather and climate extreme events in a changing climate. *Climate Change 2021: The Physical Science Basis. Contribution of Working Group I to the Sixth Assessment Report of the Intergovernmental Panel on Climate Change*, V. Masson-Delmotte, P. Zhai, A. Pirani, S. L. Connors, C. Péan, S. Berger, N. Caud, Y. Chen, L. Goldfarb, M. I. Gomis, M. Huang, K. Leitzell, E. Lonnoy, J. B. R. Matthews, T. K. Maycock, T. Waterfield, O. Yelekçi, R. Yu, and B. Zhou, Eds., Cambridge University Press, Cambridge, United Kingdom and New York, NY, USA, 1513–1766, doi:10.1017/9781009157896.014.
3. Zscheischler, J., S. Westra, B. J. Van Den Hurk, S. I. Seneviratne, P. J. Ward, A. Pitman, A. Aghakouchak, D. N. Bresch, M. Leonard, T. Wahl, and X. Zhang, 2018: Future climate risk from compound events. *Nature Climate Change*, **8 (6)**, 469–477, doi:10.1038/s41558-018-0156-3.
4. Kousky, C., 2019: The Role of Natural Disaster Insurance in Recovery and Risk Reduction. doi:10.1146/annurev-resource-100518-094028.
5. IPCC, 2023: *Climate Change 2023: Synthesis Report. Contribution of Working Groups I, II and III to the Sixth Assessment Report of the Intergovernmental Panel on Climate Change*. IPCC, Geneva, Switzerland, doi:10.59327/IPCC/AR6-9789291691647.
6. UNDRR, 2022: *Global Assessment Report on Disaster Risk Reduction 2022: Our World at Risk: Transforming Governance for a Resilient Future*. United Nations Office for Disaster Risk Reduction, Geneva, Switzerland.
7. Gallagher, J., and D. Hartley, 2017: Household Finance after a Natural Disaster: The Case of Hurricane Katrina. *American Economic Journal: Economic Policy*, **9 (3)**, 199–228, doi:10.1257/pol.20140273.
8. Kunreuther, H., and M. Useem, Eds., 2010: *Learning from Catastrophes: Strategies for Reaction and Response*. Pearson P T R, Upper Saddle River, N.J.
9. Jarzabkowski, P., K. Chalkias, E. Cacciatori, and R. Bednarek, 2023: *Disaster Insurance Reimagined: Protection in a Time of Increasing Risk*. 1st ed., Oxford University PressOxford, doi:10.1093/oso/9780192865168.001.0001.

10. Kousky, C., G. Treuer, and K. J. Mach, 2024: Insurance and climate risks: Policy lessons from three bounding scenarios. *Proceedings of the National Academy of Sciences*, **121 (48)**, e2317875 121, doi:10.1073/pnas.2317875121.

11. Pielke, R. A., J. Gratz, C. W. Landsea, D. Collins, M. A. Saunders, and R. Musulin, 2008: Normalized Hurricane Damage in the United States: 1900–2005. *Natural Hazards Review*, **9 (1)**, 29–42, doi:10.1061/(ASCE)1527-6988(2008)9:1(29).

12. Kousky, C., 2022: *Understanding Disaster Insurance: New Tools for a More Resilient Future*. Island Press, Washington.

13. California Department of Insurance, 2024: 2024 annual report of the insurance commissioner. Tech. rep., California Department of Insurance, Sacramento, CA, USA.

14. Gray, I., 2021: Hazardous simulations: Pricing climate risk in US coastal insurance markets. *Economy and Society*, **50 (2)**, 196–223, doi:10.1080/03085147.2020.1853358.

15. Kousky, C., and L. Medders, 2024: The evolution of florida's public-private approach to property insurance. Report, Florida Policy Project.

16. Hemmati, M., I. P. Gray, and S. G. Bowen, 2025: The growing void in the U.S. homeowners insurance market: Who should bear the rising cost of climate change? *npj Climate Action*, **4 (1)**, 1–7, doi:10.1038/s44168-025-00231-8.

17. Basel Committee on Banking Supervision, 2011: *Basel III: A Global Regulatory Framework for More Resilient Banks and Banking Systems*. December 2010 (rev. june 2011) ed., Basel Bank for International Settlements 2011.

18. International Monetary Fund (IMF), 2012: Macrofinancial stress testing—principles and practices. Tech. rep., International Monetary Fund.

19. Board of Governors of the Federal Reserve System, 2022: Stress tests and capital planning. https://www.federalreserve.gov/supervisionreg/stress-tests-capital-planning.htm, Accessed on 2026-03-31.

20. Battiston, S., A. Mandel, I. Monasterolo, F. Schütze, and G. Visentin, 2017: A climate stress-test of the financial system. *Nature Climate Change*, **7 (4)**, 283–288, doi:10.1038/nclimate3255.

21. Network for Greening the Financial System (NGFS), 2024: NGFS climate scenarios for central banks and supervisors—phase V. Tech. rep., Network for Greening the Financial System (NGFS).

22. Dunz, N., T. Emambakhsh, T. Hennig, M. Kaijser, C. Kouratzoglou, and C. Salleo, 2021: ECB's Economy-Wide Climate Stress Test. *SSRN Electronic Journal*, doi:10.2139/ssrn.3929178.

23. Swiss Re Institute, 2024: Sigma 1/2024: Natural catastrophes in 2023: Gearing up for today's and tomorrow's weather risks.

24. Task Force on Climate-related Financial Disclosures, 2017: Final report: Recommendations of the task force on climate-related financial disclosures. Technical report, Financial Stability Board.

25. National Association of Insurance Commissioners (NAIC), 2026: NAIC climate risk disclosure survey. https://www.insurance.ca.gov/0250-insurers/0300-insurers/0100-applications/ClimateSurvey/index.cfm, Accessed on 2026-03-31.

26. European Insurance and Occupational Pensions Authority (EIOPA), 2022: Methodological principles of insurance stress testing—climate change component. Tech. rep., European Insurance and Occupational Pensions Authority (EIOPA).

27. Abrahams, D., and T. Robustelli, 2025: Climate Change, Housing, and Homeowners Insurance in Florida: Lessons for California. http://newamerica.org/future-land-housing/briefs/insurance-in-florida-lessons-for-california/, Accessed on 2026-01-28.

28. Kaufmann, L., 2024: Florida's Home Insurance Industry May Be Worse Than Anyone Realizes. Accessed on 2026-01-28.

29. Knapp, K. R., M. C. Kruk, D. H. Levinson, H. J. Diamond, and C. J. Neumann, 2010: The International Best Track Archive for Climate Stewardship (IBTrACS). *Bulletin of the American Meteorological Society*, **91 (3)**, 363–376, doi:10.1175/2009BAMS2755.1.

30. Emanuel, K., S. Ravela, E. Vivant, and C. Risi, 2006: A Statistical Deterministic Approach to Hurricane Risk Assessment. *Bulletin of the American Meteorological Society*, **87 (3)**, S1–S5, doi:10.1175/bams-87-3-emanuel.

31. Emanuel, K., R. Sundararajan, and J. Williams, 2008: Hurricanes and global warming: Results from downscaling IPCC AR4 simulations. *Bulletin of the American Meteorological Society*, **89 (3)**, 347–367, doi:10.1175/BAMS-89-3-347.

32. Muller, J., K. Mooney, S. G. Bowen, P. J. Klotzbach, T. Martin, T. J. Philp, B. Dhruvkumar, R. S. Dixon, and S. B. Girimurugan, 2025: Normalized Hurricane Damage in the United States: 1900–2022. *Bulletin of the American Meteorological Society*, **106 (1)**, E51–E67, doi:10.1175/BAMS-D-23-0280.1.

33. Wolf, D., and K. Takeuchi, 2025: Are Building Codes an Effective Adaptation to Wind Risk? Evidence from Remotely Detected Blue Tarps.

34. Insurance Institute for Business & Home Safety, 2025: 2025 FORTIFIED home standards. Accessed on 2026-02-19.

35. Amornsiripanitch, N., S. Biswas, J. Orellana-Li, and D. Zink, 2025: Measuring flood underinsurance in the USA. *Nature Climate Change*, 1–7, doi:10.1038/s41558-025-02396-w.

36. Alabama Department of Insurance and Center for Risk and Insurance Research, 2025: Performance of IBHS FORTIFIED HomeTM construction in hurricane sally. Accessed on 2026-02-19.

37. Meiler, S., A. Ciullo, C. M. Kropf, K. Emanuel, and D. N. Bresch, 2023: Uncertainties and sensitivities in the quantification of future tropical cyclone risk. *Communications Earth & Environment*, **4 (1)**, 1–10, doi:10.1038/s43247-023-00998-w.

38. Gibson, M., and B. Hohermuth, 2025: Climate risk and insurance-linked securities: Navigating a shifting landscape. https://www.schroders.com/en-us/us/non-resident-clients/insights/climate-risk-and-insurance-linked-securities-navigating-a-shifting-landscape/, Accessed on 2026-02-24.

39. Gori, A., N. Lin, D. Chavas, M. Oppenheimer, and S. Xian, 2025: Sensitivity of tropical cyclone risk across the US to changes in storm climatology and socioeconomic growth. *Environmental Research Letters*, **20 (6)**, 064 050, doi:10.1088/1748-9326/add60d.

40. Abatzoglou, J. T., and A. P. Williams, 2016: Impact of anthropogenic climate change on wildfire across western US forests. *Proceedings of the National Academy of Sciences*, **113 (42)**, 11 770–11 775, doi:10.1073/pnas.1607171113.

41. Mishra, A., A. Arun, E. Kodra, E. Smull, O. Woolcock, T. Doe, J. Marlowe, and A. R. Ganguly, 2026: Physical climate risk creates challenges and opportunities in US municipal finance. *Nature Cities*, **3 (1)**, 11–21, doi:10.1038/s44284-025-00365-0.

42. Florida Hurricane Catastrophe Fund, 2024: Florida hurricane catastrophe fund 2024 annual report. State Board of Administration of Florida, Accessed on 2026-03-19.

43. Florida Office of Insurance Regulation, 2024: Quarterly Residential Market Share Reports. https://floir.gov/tools-and-data/residential-market-share-reports, Accessed on 2026-03-19.

44. Citizens Property Insurance Corporation, 2024: Policies in force. https://www.citizensfla.com/policies-in-force, Accessed on 2026-03-31.

45. Federal Emergency Management Agency (FEMA), 2024: FIMA NFIP redacted policies (v2). U.S. Department of Homeland Security, https://www.fema.gov/openfema-data-page/fima-nfip-redacted-policies-v2, Accessed on 2026-03-19.

46. Federal Emergency Management Agency (FEMA), 2025: OpenFEMA dataset: NFIP residential penetration rates – v1. U.S. Department of Homeland Security, https://www.fema.gov/openfema-data-page/nfip-residential-penetration-rates-v1, Accessed on 2026-03-19.

47. Citizens Property Insurance Corporation, 2024: Annual statement of the citizens property insurance corporation for the year ended december 31, 2024. Tech. rep., Citizens Property Insurance Corporation, Tallahassee, FL.

48. Congressional Research Service, 2025: National flood insurance program borrowing authority. https://www.congress.gov/crs_external_products/IN/PDF/IN10784/IN10784.43.pdf, Accessed on 2026-03-31.

49. State Board of Administration of Florida, and Florida Hurricane Catastrophe Fund, 2023: Florida hurricane catastrophe fund: 2023 annual report. Tech. rep., State Board of Administration of Florida, Tallahassee, FL.

50. Artemis.bm, 2024: Catastrophe bond and insurance-linked securities deal directory. https://www.artemis.bm/deal-directory/, Accessed on 2026-03-31.

51. Hersbach, H., B. Bell, P. Berrisford, S. Hirahara, A. Horányi, J. Muñoz-Sabater, J. Nicolas, C. Peubey, R. Radu, D. Schepers, A. Simmons, C. Soci, S. Abdalla, X. Abellan, G. Balsamo, P. Bechtold, G. Biavati, J. Bidlot, M. Bonavita, G. De Chiara, P. Dahlgren, D. Dee, M. Diamantakis, R. Dragani, J. Flemming, R. Forbes, M. Fuentes, A. Geer, L. Haimberger, S. Healy, R. J. Hogan, E. Hólm, M. Janisková, S. Keeley, P. Laloyaux, P. Lopez, C. Lupu, G. Radnoti, P. de Rosnay, I. Rozum, F. Vamborg, S. Villaume, and J.-N. Thépaut, 2020: The ERA5 global reanalysis. *Quarterly Journal of the Royal Meteorological Society*, **146 (730)**, 1999–2049, doi:10.1002/qj.3803.

52. Swart, N. C., J. N. S. Cole, V. V. Kharin, M. Lazare, J. F. Scinocca, N. P. Gillett, J. Anstey, V. Arora, J. R. Christian, S. Hanna, Y. Jiao, W. G. Lee, F. Majaess, O. A. Saenko, C. Seiler, C. Seinen, A. Shao, M. Sigmond, L. Solheim, K. von Salzen, D. Yang, and B. Winter, 2019: The Canadian Earth System Model version 5 (CanESM5.0.3). *Geoscientific Model Development*, **12 (11)**, 4823–4873, doi:10.5194/gmd-12-4823-2019.

53. Voldoire, A., D. Saint-Martin, S. Sénési, B. Decharme, A. Alias, M. Chevallier, J. Colin, J.-F. Guérémy, M. Michou, M.-P. Moine, P. Nabat, R. Roehrig, D. Salas y Mélia, R. Séférian, S. Valcke, I. Beau, S. Belamari, S. Berthet, C. Cassou, J. Cattiaux, J. Deshayes, H. Douville, C. Ethé, L. Franchistéguy, O. Geoffroy, C. Lévy, G. Madec, Y. Meurdesoif, R. Msadek, A. Ribes, E. Sanchez-Gomez, L. Terray, and R. Waldman, 2019: Evaluation of CMIP6 DECK Experiments With CNRM-CM6-1. *Journal of Advances in Modeling Earth Systems*, **11 (7)**, 2177–2213, doi:10.1029/2019MS001683.

54. EC Earth Consortium, 2019: EC-Earth-Consortium EC-Earth3 model output prepared for CMIP6 ScenarioMIP ssp245. Accessed on 2023-02-16, doi:10.22033/ESGF/CMIP6.4880.

55. Hourdin, F., C. Rio, J.-Y. Grandpeix, J.-B. Madeleine, F. Cheruy, N. Rochetin, A. Jam, I. Musat, A. Idelkadi, L. Fairhead, M.-A. Foujols, L. Mellul, A.-K. Traore, J.-L. Dufresne, O. Boucher, M.-P. Lefebvre, E. Millour, E. Vignon, J. Jouhaud, F. B. Diallo, F. Lott, G. Gastineau, A. Caubel, Y. Meurdesoif, and J. Ghattas, 2020: LMDZ6A: The Atmospheric Component of the IPSL Climate Model With Improved and Better Tuned Physics. *Journal of Advances in Modeling Earth Systems*, **12 (7)**, e2019MS001 892, doi:10.1029/2019MS001892.

56. Tatebe, H., T. Ogura, T. Nitta, Y. Komuro, K. Ogochi, T. Takemura, K. Sudo, M. Sekiguchi, M. Abe, F. Saito, M. Chikira,

S. Watanabe, M. Mori, N. Hirota, Y. Kawatani, T. Mochizuki, K. Yoshimura, K. Takata, R. O'ishi, D. Yamazaki, T. Suzuki, M. Kurogi, T. Kataoka, M. Watanabe, and M. Kimoto, 2019: Description and basic evaluation of simulated mean state, internal variability, and climate sensitivity in MIROC6. *Geoscientific Model Development*, **12 (7)**, 2727–2765, doi:10.5194/gmd-12-2727-2019.

57. Aznar-Siguan, G., and D. N. Bresch, 2019: CLIMADA v1: A global weather and climate risk assessment platform. *Geoscientific Model Development*, **12 (7)**, 3085–3097, doi:10.5194/gmd-12-3085-2019.

58. IPCC, 2012: *Managing the Risks of Extreme Events and Disasters to Advance Climate Change Adaptation. A Special Report of Working Groups I and II of the Intergovernmental Panel on Climate Change [Field, C.B., V. Barros, T.F. Stocker, D. Qin, D.J. Dokken, K.L. Ebi, M.D.* doi:10.1017/CBO9781139177245.

59. Holland, G., 2008: A revised hurricane pressure-wind model. *Monthly Weather Review*, **136 (9)**, 3432–3445, doi:10.1175/2008MWR2395.1.

60. Eberenz, S., D. Stocker, T. Röösli, and D. N. Bresch, 2020: Asset exposure data for global physical risk assessment. *Earth System Science Data*, **12 (2)**, 817–833, doi:10.5194/essd-12-817-2020.

61. Eberenz, S., S. Lüthi, and D. N. Bresch, 2021: Regional tropical cyclone impact functions for globally consistent risk assessments. *Natural Hazards and Earth System Sciences*, **21 (1)**, 393–415, doi:10.5194/nhess-21-393-2021.

62. Gori, A., 2025: Tropical Cyclone Synthetic Hazard and Damage Simulations. DesignSafe-CI, Accessed on 2026-02-12, doi:10.17603/ds2-0jkm-h487.

63. Smith, A. B., and R. W. Katz, 2013: US billion-dollar weather and climate disasters: Data sources, trends, accuracy and biases. *Natural Hazards*, **67 (2)**, 387–410, doi:10.1007/s11069-013-0566-5.

64. Smith, A. B., and J. L. Matthews, 2015: Quantifying uncertainty and variable sensitivity within the US billion-dollar weather and climate disaster cost estimates. *Natural Hazards*, **77 (3)**, 1829–1851, doi:10.1007/s11069-015-1678-x.

65. Florida Office of Insurance Regulation, 2026: Catastrophe Reporting. https://floir.gov/tools-and-data/catastrophe-reporting, Accessed on 2026-03-19.

66. National Flood Insurance Program, 2026: Historical NFIP Claims Information and Trends. https://www.floodsmart.gov/historical-nfip-claims-information-and-trends, Accessed on 2026-03-19.

67. Federal Emergency Management Agency (FEMA), 2026: Disaster Declarations Summaries - v2. U.S. Department of Homeland Security, https://www.fema.gov/openfema-data-page/disaster-declarations-summaries-v2, Accessed on 2026-03-19.

68. Camargo, S. J., 2013: Global and regional aspects of tropical cyclone activity in the CMIP5 models. *Journal of Climate*, **26 (24)**, 9880–9902, doi:10.1175/JCLI-D-12-00549.1.

69. Siguan, G. A., D. N. Bresch, S. Eberenz, J. Hartman, M. Perus, T. Röösli, D. Stocker, V. Bozzini, C. B. Steinmann, E. Mühlhofer, R. Bungerer, I. J. Sauer, S. Lüthi, P. M. M. Kam, S. Meiler, A. Ciullo, T. Vogt, B. P. Guillod, C. M. Kropf, E. Schmid, C. Fairless, J. Wüthrich, Z. Stalhandske, Y. Yu, L. Riedel, R. Portmann, N. Colombi, L. Villiger, T. Schmid, L. Severino, S. Juhel, V. Gebhart, and D. Araya, 2025: CLIMADA Core Python Package. Zenodo, Accessed on 2026-03-23, doi:10.5281/zenodo.17233409.

70. Meiler, S., 2026: Simonameiler/systemic_insurance_risk_fl_pub: V1.0.0. Zenodo, Accessed on 2026-03-31, doi:10.5281/zenodo.19361128.

71. US Bureau of Labor Statistics, 2026: Consumer Price Index for All Urban Consumers (CPI-U). https://data.bls.gov/PDQWeb/cu, Accessed on 2026-03-19.

Acknowledgements

Funding

SM acknowledges support from the Swiss National Science Foundation Postdoc.Mobility Fellowship (P500PN_222189) and from the Stanford Urban Resilience Initiative. NSD acknowledges support from Stanford University.

The development of the risk propagation model underlying this study was initiated in collaboration with the Insurance Policy Advisory Committee (IPAC) of the U.S. Federal Reserve System, for which Simona Meiler developed an initial flow-of-risk modeling approach. We thank members of the IPAC Property Insurance Working Group for valuable discussions and insights that informed the conceptual design of the model. The analysis presented here represents independent academic work and does not reflect the views of the Federal Reserve System or its committees.

Author contributions statement

Conceptualization: SM, SIJ
Methodology: SM
Visualization: SM

Datasets: SM, SIJ, KE
Writing - original draft: SM
Writing - review & editing: SM, SIJ, KE, NSD, JWB

Competing interests

All authors (SM, SIJ, KE, NSD, JWB) declare no competing interests. Kerry Emanuel is on the board of Trusted Resource Underwriters, which insures homeowners in Florida.

Supplementary Information for article "Stress testing insurance market stability under climate risk"

Simona Meiler[1,*], Steven I. Jackson[2], Kerry Emanuel[3], Noah S. Diffenbaugh[4], and Jack W. Baker[1]

[1]Civil and Environmental Engineering, Stanford University, CA, USA
[2]American Academy of Actuaries, Washington, DC, USA
[3]Lorenz Center, Massachusetts Institute of Technology, Cambridge, Massachusetts, USA
[4]Earth System Science, Stanford University, CA, USA
[*]Corresponding author: simona@simonameiler.ch

Supplementary Methods

Estimation of insured loss fractions for tropical cyclone events

To estimate the fraction of economic losses covered by insurance for tropical cyclone events, we reconstruct empirical relationships between insured and total economic losses using Florida-specific data. Our approach follows the methodology of the U.S. Billion-Dollar Weather and Climate Disaster Database (1, 2), in which total economic losses are inferred from insured losses, National Flood Insurance Program (NFIP) payouts, and federal disaster assistance.

Total economic losses are estimated as:

$$L_{\text{econ}} = 2 \cdot L_{\text{insured}} + L_{\text{NFIP}} + L_{\text{FDA}}, \tag{1}$$

where L_{insured} denotes insured losses reported by the Florida Office of Insurance Regulation (OIR), L_{NFIP} represents NFIP payouts, and L_{FDA} denotes federal disaster assistance. Following (1), the factor of two applied to insured losses accounts for uninsured private losses.

Because the treatment of federal disaster assistance in economic loss accounting is uncertain, we compute two estimates of economic losses: one including L_{FDA} and one excluding it. The insured fraction is then calculated for both formulations as:

$$f_{\text{insured}} = \frac{L_{\text{insured}}}{L_{\text{econ}}}, \tag{2}$$

and averaged across both estimates.

We compile insured loss data from the Florida OIR for hurricane-related losses (2017–2020 and 2022–2024) (3), complemented by NFIP payout data from FEMA's Floodsmart database (4) and federal disaster assistance from FEMA disaster summaries (5). All monetary values are converted to 2024 USD using the Consumer Price Index (CPI-U) from the U.S. Bureau of Labor Statistics (6).

Estimated insured shares vary substantially across years (table S1), ranging from approximately 10% in low-loss years to nearly 50% in high-loss years. Years with large economic losses (exceeding $25 billion) consistently exhibit insured shares above 40%, indicating that insurance penetration increases with event severity.

Averaging across all years, estimation approaches, and subsets of high-loss years yields an overall mean insured share of 38.9%. Given that the stress-test scenarios considered in this study focus on severe hurricane events and loss years, we adopt a representative insured fraction of 40% for wind-related losses. To account for uncertainty, this fraction is implemented as a Beta distribution centered at 0.4 (Beta(4,6)), reflecting variability around the empirical mean while emphasizing higher insured shares in large-loss events.

Table S1: Insured and estimated economic losses and resulting insured shares for Florida hurricane events (2017–2024). Economic losses are estimated using formulations including and excluding federal disaster assistance (FDA). All values are converted to 2024 USD.

Year	Insured losses	Est econ loss (incl. FDA)	f_{insured} (incl.)	Est econ loss (excl. FDA)	f_{insured} (excl.)
2017	28,159,458,046	60,750,223,673	46.35%	57,644,860,280	48.85%
2018	11,472,501,417	26,081,530,262	43.99%	23,251,364,093	49.34%
2019	23,342,615	198,468,914	11.76%	80,793,892	28.89%
2020	699,057,474	2,041,794,621	34.24%	1,783,712,209	39.19%
2021	—	—	—	—	—
2022	23,914,182,689	56,175,193,964	42.57%	53,075,926,756	45.06%
2023	318,470,377	1,754,055,340	18.16%	1,315,565,662	24.21%
2024	7,466,073,319	25,060,543,556	29.79%	22,700,454,161	32.89%
Mean			32.41%		38.35%
Median			34.24%		39.19%
High-loss mean ($>$ \$25B)			40.68%		44.03%

Table S2: Definitions of systemic risk metrics used in the main text and Supplementary Information.

Metric	Unit	Definition	Used in
Loss decomposition			
Total loss	USD	Aggregate economic tropical cyclone loss before redistribution across insurance and public backstop layers.	Table 1, Tables S2–S3, Figs. 2, 6
Insured wind – private	USD	Wind-related losses allocated to private admitted-market insurers in the initial risk-absorption layer.	Table 1, Tables S2–S3, Fig. 2
Citizens wind	USD	Wind-related losses allocated to Citizens in the initial risk-absorption layer.	Table 1, Tables S2–S3, Fig. 2
Insured flood – NFIP	USD	Flood-related losses allocated to the NFIP.	Table 1, Tables S2–S3, Fig. 2
Un/underinsured wind	USD	Wind-related damages not covered by private insurance or Citizens because of un- or underinsurance.	Table 1, Tables S2–S3, Fig. 2
Un/underinsured flood	USD	Flood-related damages not covered by the NFIP because of un- or underinsurance.	Table 1, Tables S2–S3, Fig. 2
Household burden	USD	Combined un/underinsured wind and flood losses.	Fig. 2
Insured / uninsured share	%	Share of total loss that is insured or un/underinsured.	Fig. 2
Institutional stress and public burden			
FHCF shortfall	USD	Unrecovered wind losses resulting when the FHCF season-wide payout cap binds.	Table 1, Tables S2–S3, Figs. 2, S2
FIGA residual	USD	Residual deficit remaining after insurer insolvencies are absorbed through the FIGA, subject to its assessment limits.	Table 1, Tables S2–S3, Figs. 2, S2
Citizens deficit	USD	Residual deficit remaining after Citizens' surplus and assessment capacity are exhausted.	Table 1, Tables S2–S3, Figs. 2, S2
NFIP Treasury borrowing	USD	Portion of Florida-attributable NFIP losses financed through borrowing from the U.S. Treasury once NFIP fund balances are insufficient.	Table 1, Tables S2–S3, Figs. 2, S2
Total public burden	USD	The sum of FHCF shortfall, FIGA residual, Citizens deficit, and NFIP Treasury borrowing.	Table 1, Tables S2–S3, Figs. 2, 6
Capital depletion and default outcomes			
Private defaults	#	Number of private insurer entities that become insolvent under a simulated event or season after modeled capital depletion.	Table S2, Figs. 3–4, S2
Largest single-entity deficit	USD	Maximum capital shortfall of any one insurer entity in a simulated event or season.	Table S2, Figs. 3–4, Fig. S2
Stress ratios			
FHCF utilization factor	ratio	Share of the FHCF season-wide statutory payout capacity utilized in a given scenario or simulation. A value of 1 indicates that the cap is fully used.	Table S2
Citizens assessment stress factor	ratio	Citizens' deficit divided by its maximum assessment capacity (Tier 1 + Tier 2). Values above 1 indicate that the funding need exceeds statutory capacity.	Table S2
FIGA stress factor	ratio	Insolvency-related deficit relative to FIGA's effective maximum assessment capacity. Values above 1 indicate exceedance of capacity.	Table S2
NFIP Florida stress factor	ratio	Florida-attributable NFIP claims paid divided by Florida NFIP annual premium volume.	Table S2
Probabilistic exceedance metrics			
Defaults > 10	annual probability (%)	Probability that more than ten private insurers default in a simulated tropical cyclone season.	Figs. 3–5, Table S4
Single deficit $>$ \$1B	annual probability (%)	Probability that the largest single-company deficit exceeds USD 1 billion in a simulated season.	Figs. 3–5, Table S4
FHCF $> 100\%$ cap	annual probability (%)	Probability that modeled FHCF payouts reach or exceed the season-wide statutory cap.	Figs. 3–5, Table S4
FIGA $> 100\%$ capacity	annual probability (%)	Probability that FIGA funding needs exceed its statutory assessment capacity.	Figs. 3–5, Table S4
Citizens $> 100\%$ capacity	annual probability (%)	Probability that Citizens' deficit exceeds its assessment capacity.	Figs. 3–5, Table S4
NFIP $> 200\%$ annual premium	annual probability (%)	Probability that Florida-attributable NFIP losses exceed twice Florida NFIP annual premium income.	Figs. 3–5, Table S4
Public burden $> 1\%$ Florida GDP	annual probability (%)	Probability that total public burden exceeds 1% of Florida's GDP in a simulated season.	Figs. 3–5, Table S4
Public burden $> 10\%$ Florida GDP	annual probability (%)	Probability that total public burden exceeds 10% of Florida's GDP in a simulated season.	Figs. 3–5, Table S4

Table S3: Scenario-based loss decomposition and institutional stress outcomes for Florida hurricane events. Results are reported as mean values across stochastic realizations, with uncertainty ranges in parentheses indicating the 5th–95th percentiles. Metric definitions are provided in table S2.

Metric	Great Miami	Andrew	Lake Okeechobee	Irma	Great Miami then Andrew	Double Great Miami	Double Irma
Loss decomposition							
Total loss (USD)	170.4B (170.4-170.4B)	114.2B (114.2-114.2B)	156.9B (156.9-156.9B)	32.0B (32.0-32.0B)	266.5B (266.5-266.5B)	321.1B (321.1-321.1B)	62.4B (62.4-62.4B)
Insured wind – private (USD)	36.9B (20.2-56.1B)	29.0B (14.0-46.4B)	16.3B (4.3-31.6B)	6.0B (2.8-9.5B)	61.4B (35.6-90.6B)	69.3B (42.7-98.1B)	11.5B (7.4-15.9B)
Citizens wind (USD)	10.3B (4.9-17.1B)	10.3B (4.6-17.7B)	2.6B (0.7-5.1B)	0.5B (0.2-0.7B)	18.8B (9.7-30.0B)	19.4B (10.5-30.5B)	0.9B (0.6-1.2B)
Insured flood – NFIP (USD)	15.0B (4.9-27.7B)	4.9B (0.5-12.9B)	17.0B (10.5-22.4B)	2.6B (1.3-4.0B)	19.8B (9.4-31.9B)	28.1B (16.1-41.4B)	5.2B (3.6-6.7B)
Un/Underinsured wind (USD)	72.2B (42.5-101.3B)	60.5B (37.8-84.5B)	28.3B (7.6-55.4B)	9.7B (4.7-14.9B)	122.9B (84.4-165.0B)	136.7B (96.0-180.5B)	18.7B (12.8-25.5B)
Un/Underinsured flood (USD)	35.9B (11.4-66.8B)	9.4B (0.9-24.7B)	92.6B (57.3-121.9B)	13.3B (6.5-20.1B)	43.7B (20.5-70.7B)	67.7B (38.5-100.1B)	26.1B (18.0-33.8B)
Institutional stress							
Total public burden (USD)	26.1B (15.4-38.8B)	11.7B (4.1-22.3B)	18.4B (16.6-20.9B)	0.2B (0.0-0.8B)	51.0B (28.7-74.0B)	65.4B (42.7-88.3B)	3.1B (2.1-4.0B)
FHCF shortfall (USD)	1.7B (0.0-8.0B)	0.0B (0.0-0.0B)	0.0B (0.0-0.0B)	0.0B (0.0-0.0B)	5.6B (0.0-11.6B)	8.0B (0.0-12.7B)	0.0B (0.0-0.0B)
FIGA residual (USD)	7.0B (3.2-13.4B)	4.2B (1.1-10.0B)	3.3B (0.0-8.8B)	0.1B (0.0-0.7B)	15.8B (6.2-27.7B)	19.1B (8.5-31.1B)	1.3B (0.1-2.8B)
Citizens deficit (USD)	5.8B (3.1-11.4B)	5.2B (1.9-11.9B)	1.6B (0.0-4.0B)	0.0B (0.0-0.0B)	13.2B (4.7-24.1B)	13.6B (5.5-24.7B)	0.0B (0.0-0.3B)
NFIP treasury borrowing (USD)	11.5B (1.4-24.3B)	2.2B (0.0-9.4B)	13.6B (7.1-18.9B)	0.1B (0.0-0.5B)	16.4B (6.0-28.5B)	24.7B (12.7-38.0B)	1.8B (0.2-3.3B)
Capital & default assessment							
Private defaults (#)	18 (15-22)	16 (12-20)	13 (0-18)	5 (0-11)	21 (18-23)	22 (19-24)	12 (8-14)
Largest single-entity deficit (USD)	1.9B (1.1-3.3B)	1.2B (0.4-2.8B)	1.0B (0.0-2.4B)	0.1B (0.0-0.4B)	3.8B (1.6-6.8B)	4.6B (2.2-7.5B)	0.6B (0.2-1.0B)
Stress ratios							
FHCF utilization factor	0.79 (0.20-1.00)	0.74 (0.25-0.93)	0.02 (0.00-0.08)	0.00 (0.00-0.00)	0.98 (0.87-1.00)	0.98 (0.92-1.00)	0.00 (0.00-0.01)
Citizens assessment stress factor	6.46 (3.43-12.64)	5.83 (2.16-13.26)	1.74 (0.00-4.46)	0.00 (0.00-0.00)	14.67 (5.26-26.77)	15.13 (6.07-27.40)	0.06 (0.00-0.29)
FIGA stress factor	0.95 (0.91-0.98)	0.88 (0.74-0.97)	0.77 (0.00-0.97)	0.17 (0.00-0.67)	0.98 (0.95-0.99)	0.98 (0.97-0.99)	0.70 (0.23-0.89)
NFIP Florida stress factor	10.73 (3.49-19.86)	3.54 (0.35-9.23)	12.19 (7.56-16.02)	1.90 (0.95-2.85)	14.20 (6.74-22.89)	20.13 (11.54-29.68)	3.71 (2.58-4.79)

Table S4: Loss decomposition and public institutional burden across climate and policy scenarios. Values show expected annual losses and institutional burdens under present-day baseline conditions, future climate scenarios (2050 and 2100 under SSP2-4.5 and SSP5-8.5), and illustrative market and policy interventions evaluated under present-day climate forcing. Values are reported as means in billion USD with uncertainty ranges (10th–90th percentile) in parentheses.

Metric (USD B)	Baseline	2050 SSP2-4.5	2050 SSP5-8.5	2100 SSP2-4.5	2100 SSP5-8.5	Market Exit	Insurance Penetration	Building Codes
Loss decomposition								
Total loss	19.3 (0.0–37.8)	31.5 (15.3–45.5)	34.9 (17.6–55.6)	41.9 (18.3–50.0)	59.2 (22.2–104.2)	19.3 (0.0–37.8)	19.3 (0.0–37.9)	19.3 (0.0–38.0)
Insured wind – private	5.5 (0.0–11.6)	13.9 (6.7–19.9)	15.4 (7.8–24.3)	18.5 (8.1–22.1)	26.2 (9.8–46.0)	4.7 (0.0–9.8)	8.1 (0.0–17.3)	3.8 (0.0–8.1)
Citizens wind	1.1 (0.0–1.8)	2.6 (1.3–3.8)	2.9 (1.5–4.6)	3.4 (1.5–4.1)	4.7 (1.8–8.6)	1.9 (0.0–3.5)	1.7 (0.0–2.8)	0.8 (0.0–1.2)
Insured flood – NFIP	0.6 (0.0–0.9)	1.5 (0.8–2.3)	1.7 (0.8–2.7)	1.9 (0.9–2.3)	2.7 (1.0–5.0)	0.6 (0.0–0.9)	1.7 (0.0–2.4)	0.5 (0.0–0.7)
Un/underinsured wind	9.7 (0.0–19.8)	7.3 (3.6–10.8)	8.3 (4.1–13.1)	9.9 (4.3–11.8)	14.0 (5.2–24.5)	9.7 (0.0–19.8)	6.5 (0.0–13.4)	11.7 (0.0–23.8)
Un/underinsured flood	2.4 (0.0–3.9)	6.2 (2.9–8.8)	6.6 (3.4–10.8)	8.2 (3.5–9.6)	11.5 (4.3–20.1)	2.4 (0.0–3.9)	1.3 (0.0–2.0)	2.6 (0.0–4.1)
Institutional stress								
Total public burden	2.7 (0.0–1.7)	7.1 (3.3–11.0)	7.8 (4.0–13.9)	9.6 (4.1–12.3)	14.9 (5.1–29.7)	3.1 (0.0–2.7)	5.1 (0.0–2.5)	1.6 (0.0–0.5)
FHCF shortfall	0.3 (0.0–0.0)	1.0 (0.4–1.6)	1.1 (0.6–2.1)	1.5 (0.6–2.0)	2.5 (0.8–5.1)	0.4 (0.0–0.0)	0.7 (0.0–0.0)	0.2 (0.0–0.0)
FIGA residual	1.3 (0.0–1.0)	3.4 (1.6–5.2)	3.8 (1.9–6.6)	4.7 (2.0–6.0)	7.3 (2.5–14.3)	1.1 (0.0–0.7)	2.0 (0.0–1.0)	0.8 (0.0–0.3)
Citizens deficit	0.7 (0.0–0.7)	1.8 (0.9–2.8)	2.0 (1.0–3.4)	2.4 (1.0–3.0)	3.5 (1.3–6.9)	1.3 (0.0–2.1)	1.2 (0.0–1.6)	0.5 (0.0–0.2)
NFIP Treasury borrowing	0.3 (0.0–0.0)	0.8 (0.4–1.4)	0.9 (0.5–1.7)	1.0 (0.4–1.4)	1.7 (0.6–3.4)	0.3 (0.0–0.0)	1.2 (0.0–0.0)	0.2 (0.0–0.0)

Table S5: Probabilistic exceedance of systemic insurance stress thresholds across climate and policy scenarios. Annual exceedance probabilities (percent) of systemic stress thresholds for private insurers, public and quasi-public institutions, and aggregate fiscal impact, estimated from 10000 simulated tropical cyclone seasons. Results are shown for present-day conditions, mid-century (2050) and end-of-century (2100) climate scenarios under SSP2-4.5 and SSP5-8.5, as well as illustrative market and policy interventions evaluated under present-day climate forcing. Values denote mean probabilities, with uncertainty ranges (10th–90th percentile) in parentheses.

Metric (%)	Baseline	2050 SSP2-4.5	2050 SSP5-8.5	2100 SSP2-4.5	2100 SSP5-8.5	Market Exit	Insurance Penetration	Building Codes
Defaults > 10	11.4 (10.9-11.8)	17.7 (12.6-20.6)	18.8 (13.1-22.2)	20.2 (13.5-21.3)	22.7 (14.6-27.3)	10.3 (9.9-10.7)	9.7 (9.3-10.0)	9.2 (8.8-9.6)
Single Deficit > $1B	7.2 (6.9-7.5)	11.5 (7.9-14.2)	12.2 (8.6-15.9)	13.5 (8.8-15.1)	16.6 (9.9-22.8)	6.5 (6.2-6.8)	8.2 (7.9-8.6)	5.6 (5.3-5.9)
FHCF > 100% Cap	0.8 (0.7-0.9)	0.9 (0.7-1.1)	1.0 (0.7-1.2)	1.0 (0.7-1.1)	1.2 (0.8-1.6)	0.7 (0.6-0.8)	1.2 (1.0-1.3)	0.5 (0.4-0.6)
FIGA > 100% Capacity	13.6 (13.2-14.1)	22.1 (15.1-27.5)	23.3 (16.6-30.9)	26.0 (17.0-29.4)	32.3 (19.0-45.3)	12.8 (12.3-13.2)	13.4 (13.0-13.9)	11.5 (11.1-11.9)
Citizens > 100% Capacity	9.5 (9.2-9.9)	15.1 (10.4-18.8)	16.1 (11.2-20.8)	17.3 (11.5-19.4)	21.0 (12.6-29.5)	13.0 (12.6-13.4)	11.8 (11.3-12.2)	7.9 (7.6-8.3)
NFIP > 200% Annual Premium	5.0 (4.8-5.3)	5.9 (4.4-6.9)	6.1 (4.6-7.5)	6.6 (4.7-7.2)	7.7 (5.0-10.0)	5.0 (4.8-5.3)	9.3 (8.9-9.7)	4.0 (3.7-4.2)
Public Burden > 1% FL GDP	3.7 (3.5-3.9)	4.3 (3.2-5.1)	4.5 (3.4-5.5)	4.9 (3.4-5.3)	5.6 (3.7-7.3)	4.3 (4.0-4.5)	5.6 (5.3-5.9)	2.4 (2.2-2.6)
Public Burden > 10% FL GDP	0.1 (0.1-0.2)	0.2 (0.1-0.2)	0.2 (0.1-0.2)	0.2 (0.1-0.2)	0.2 (0.1-0.3)	0.2 (0.1-0.3)	0.7 (0.6-0.8)	0.0 (0.0-0.1)

Table S6: Sensitivity of model outputs to the insured wind loss fraction. Mean values (in $B; insurer defaults reported as counts) for each output metric across five fixed values of the insured wind fraction f. The table also reports the relative change compared to the reference case ($f = 0.4$, the mean of the baseline Beta(4, 6) prior) and the approximate log–log elasticity ε evaluated at $f = 0.4$. Metrics with $\varepsilon \approx 0$ are invariant to the insured fraction by construction; $\varepsilon = 1$ indicates proportional scaling; and $\varepsilon > 1$ indicates amplification through the insurance system.

	Mean value ($B)					Change vs. f=0.4				
Metric	f=0.1	f=0.2	f=0.3	f=0.4	f=0.5	$\Delta_{0.1}$	$\Delta_{0.2}$	$\Delta_{0.3}$	$\Delta_{0.5}$	ε
Loss decomposition										
Wind insured — private	1.36	2.72	4.08	5.44	6.80	-75%	-50%	-25%	+25%	+1.00
Wind insured — Citizens	0.27	0.53	0.80	1.07	1.34	-75%	-50%	-25%	+25%	+1.00
Wind un/underinsured	10.26	9.12	7.98	6.84	5.70	+50%	+33%	+17%	-17%	-0.66
Institutional stress										
FHCF shortfall	0.02	0.10	0.22	0.36	0.50	-95%	-74%	-39%	+39%	+1.60
FIGA residual deficit	0.15	0.46	0.84	1.27	1.72	-88%	-64%	-34%	+36%	+1.40
Citizens residual deficit	0.12	0.29	0.49	0.71	0.94	-84%	-60%	-31%	+32%	+1.28
Capital / defaults										
Insurer defaults (count)	0.8186	1.4122	1.8586	2.1992	2.4831	-63%	-36%	-15%	+13%	+0.57
Largest entity deficit	0.05	0.13	0.22	0.32	0.43	-84%	-59%	-31%	+32%	+1.25

Table S7: Relative contributions of hazard variability and parameter uncertainty to model output variance. Values of η^2 from a one-way ANOVA applied to a nested Monte Carlo design (300 seasons $\times$ 50 independent parameter draws per season), measuring the fraction of total variance attributable to between-season hazard differences versus within-season parameter uncertainty. $\eta^2 \geq 0.95$ for all non-flood metrics indicates that hazard realization dominates; the lower values for flood-linked metrics reflect the wind/water share Beta prior, which controls how much total damage is routed to NFIP versus private wind coverage.

Metric	η^2 (hazard)	$1 - \eta^2$ (parameters)
Loss decomposition		
Private insurer wind losses	0.976	0.024
Citizens wind losses	0.964	0.036
NFIP flood (insured)	0.772	0.228
Un/underinsured wind	0.977	0.023
Un/underinsured flood	0.749	0.251
Institutional stress		
FHCF shortfall	0.944	0.056
FIGA residual deficit	0.965	0.035
Citizens residual deficit	0.954	0.046
NFIP Treasury borrowing	0.734	0.266
Defaults		
Insurer defaults (count)	0.990	0.010
Largest entity deficit	0.961	0.039

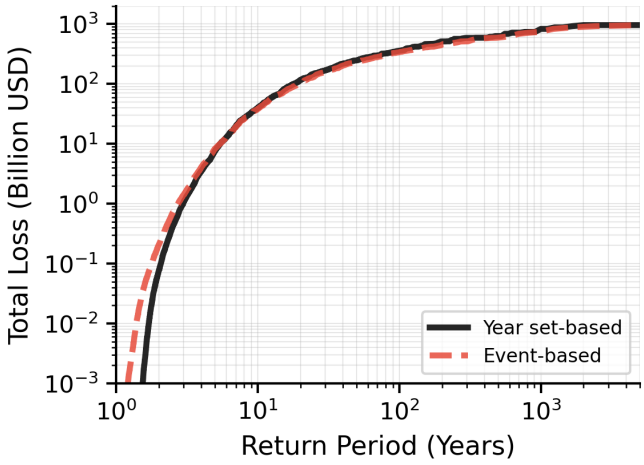

Fig. S1: Return period curves for total tropical cyclone losses in Florida. Event-based losses (red dashed line) and seasonal aggregate losses (solid black line) are shown. Event-based return periods are derived from the empirical exceedance distribution of single events in the historical tropical cyclone event set (8800 events covering 1980–2023; Section Tropical cyclone track data). Seasonal return periods are computed from the empirical exceedance distribution of aggregate losses across simulated 10 000 tropical cyclone years (Section Hazard and loss modeling).

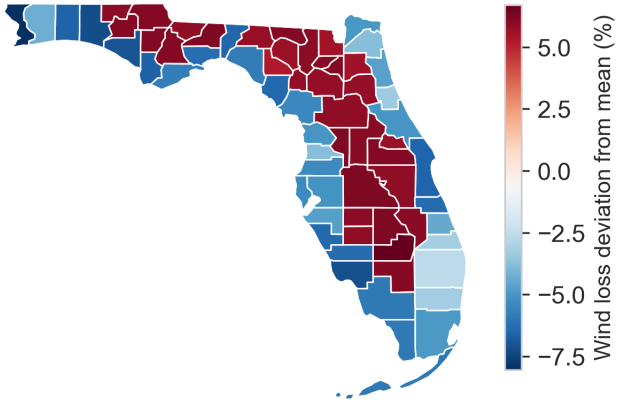

Fig. S2: County-level deviation in wind loss attribution across Florida. Percentage-point deviation of county-specific wind shares from the state-wide mean, derived from the upper 95th percentile of the compound hazard distribution in the synthetic tropical cyclone event set (cf. Methods Wind and flood loss estimation). Positive values indicate wind-dominated counties; negative values indicate relatively stronger flood contributions.